

The SURvey for Pulsars and Extragalactic Radio Bursts II: New FRB discoveries and their follow-up

S. Bhandari,^{1,2,3}* E. F. Keane,^{4,1,2} E. D. Barr,^{9,1,2} A. Jameson,^{1,2} E. Petroff,^{5,1,2,3}
 S. Johnston,³ M. Bailes,^{1,2} N. D. R. Bhat,^{2,10} M. Burgay,¹¹ S. Burke-Spolaor,^{6,7}
 M. Caleb,^{2,12} R. P. Eatough,⁹ C. Flynn,^{1,2} J. A. Green,³ F. Jankowski,^{1,2} M. Kramer,^{9,15}
 V. Venkatraman Krishnan,^{1,2} V. Morello,^{9,1} A. Possenti,¹¹ B. Stappers,¹⁵ C. Tiburzi,¹⁶
 W. van Straten,^{1,17} I. Andreoni,^{1,2,8} T. Butterley,²⁹ P. Chandra,¹³ J. Cooke,¹ A. Corongiu,¹¹
 D. M. Coward,²¹ V. S. Dhillon,^{15,27} R. Dodson,²⁴ L. K. Hardy,¹⁴ E. J. Howell,²¹
 P. Jaroenjittichai,³⁰ A. Klotz,^{22,23} S. P. Littlefair,¹⁵ T. R. Marsh,²⁸ M. Mickaliger,¹⁵
 T. Muxlow,¹⁵ D. Perrodin,¹¹ T. Pritchard,¹ U. Sawangwit,³⁰ T. Terai,²⁵ N. Tominaga,^{19,31}
 P. Torne,⁹ T. Totani,²⁰ A. Trois,¹¹ D. Turpin,^{22,23} Y. Niino,²⁶ R. W. Wilson,²⁹
 The ANTARES Collaboration. †

Accepted XXX. Received YYY; in original form ZZZ

ABSTRACT

We report the discovery of four Fast Radio Bursts (FRBs) in the ongoing SURvey for Pulsars and Extragalactic Radio Bursts (SUPERB) at the Parkes Radio Telescope: FRBs 150610, 151206, 151230 and 160102. Our real-time discoveries have enabled us to conduct extensive, rapid multi-messenger follow-up at 12 major facilities sensitive to radio, optical, X-ray, gamma-ray photons and neutrinos on time scales ranging from an hour to a few months post-burst. No counterparts to the FRBs were found and we provide upper limits on afterglow luminosities. None of the FRBs were seen to repeat. Formal fits to all FRBs show hints of scattering while their intrinsic widths are unresolved in time. FRB 151206 is at low Galactic latitude, FRB 151230 shows a sharp spectral cutoff, and FRB 160102 has the highest dispersion measure ($DM = 2596.1 \pm 0.3 \text{ pc cm}^{-3}$) detected to date. Three of the FRBs have high dispersion measures ($DM > 1500 \text{ pc cm}^{-3}$), favouring a scenario where the DM is dominated by contributions from the Intergalactic Medium. The slope of the Parkes FRB source counts distribution with fluences $> 2 \text{ Jy ms}$ is $\alpha = -2.2^{+0.6}_{-1.2}$ and still consistent with a Euclidean distribution ($\alpha = -3/2$). We also find that the all-sky rate is $1.7^{+1.5}_{-0.9} \times 10^3 \text{ FRBs}/(4\pi \text{ sr})/\text{day}$ above $\sim 2 \text{ Jy ms}$ and there is currently no strong evidence for a latitude-dependent FRB sky-rate.

Key words: surveys – radiation mechanisms: general – intergalactic medium – radio continuum: general – methods: observational – methods: data analysis

1 INTRODUCTION

High-time resolution studies of the radio Universe have led to the discovery of Fast Radio Bursts (FRBs). First seen in 2007 in archival Parkes radio telescope data (Lorimer et al. 2007), FRBs have dispersion measures (DMs) which can exceed the Milky Way contribution by more than an order of magnitude (Petroff et al. 2016) and typically have durations of a few milliseconds. In the past couple of years

the discovery rate has accelerated — including those reported here, there are now 31 FRBs known — which include discoveries from the Green Bank Telescope (GBT), the Parkes radio telescope, the Arecibo Observatory, the upgraded Molonglo synthesis telescope (UTMOST) and the Australian SKA Pathfinder (ASKAP) (Lorimer et al. 2007; Keane et al. 2012; Thornton et al. 2013; Burke-Spolaor & Bannister 2014; Spitler et al. 2014; Petroff et al. 2015a; Ravi et al. 2015; Champion et al. 2016; Masui et al. 2015; Keane et al. 2016; Ravi et al. 2016; Petroff et al. 2017; Caleb et al. 2017; Bannister et al. 2017).

The origin of these bursts is currently unknown, with leading

*Email: shivanibhandari58@gmail.com

†Full author list and affiliations included at the end of the paper

theories suggesting giant flares from magnetars (Thornton et al. 2013; Pen & Connor 2015), compact objects located in young expanding supernovae (Connor et al. 2016; Piro 2016) and supergiant pulses from extragalactic neutron stars (Cordes & Wasserman 2016) as possible progenitors. Other theories involve cataclysmic models including neutron star mergers (Totani 2013) and “blitzars” occurring when a neutron star collapses to a black hole (Falcke & Rezzolla 2014).

Independent of the physical mechanism/process, an FRB may leave an afterglow through interaction with the surrounding medium. Yi et al. (2014) have estimated FRB afterglow luminosities, using standard GRB afterglow models in radio, optical and X-ray bands, assuming a plausible range of total kinetic energies and redshifts. Lyutikov & Lorimer (2016) have discussed possible electromagnetic counterparts for FRBs; searching for such counterparts is thus one strategy for localising FRB host galaxies. Chatterjee et al. (2017) directly localised the repeating FRB 121102 (Spitler et al. 2016) using the Karl G. Jansky Very Large Array Telescope (VLA) and identified its host to be a dwarf galaxy at a redshift $z \sim 0.2$ (Tendulkar et al. 2017). The host is co-located with a persistent variable radio source. Additionally, the radio follow-ups of FRB 131104 (Shannon & Ravi 2016) and FRB 150418 (Keane et al. 2016; Johnston et al. 2017) have shown the presence of variable radio emission from Active Galactic Nuclei (AGN) in the fields of FRBs.

The SURvey for Pulsars and Extragalactic Radio Bursts (SUPERB) is currently ongoing at the Parkes radio telescope and is described in detail in Keane et al. (2017), hereafter Paper 1. Initial results from the SUPERB survey have already been published elsewhere — this includes investigations into radio frequency interference (RFI) at the Parkes site (Petroff et al. 2015c), the discovery of FRB 150418 (Keane et al. 2016) and the discovery of new pulsars (Paper 1). Here we report further results from the survey, in particular the discovery of four new FRBs —150610, 151206, 151230 and 160102 — as well as the multi-messenger follow-up of the four FRBs. In §2, we provide an overview of the observations and techniques for the FRB search. Next we present the new FRB discoveries and their properties in §3. FRB multi-messenger follow-up observations and their results are described in §4. Finally, in §5 and §6 we present our conclusions and discuss the implications of our results.

2 OBSERVATIONS AND TECHNIQUES

The full details of the SUPERB observing system and analysis setup can be found in Paper 1; here we briefly summarise the key points relevant to this work. Real-time searches are conducted for both transient and periodic signals in the incoming data. These data are also searched offline through a more rigorous process which operates slower than real time. These two streams are called the “Fast” (F) and “Thorough” (T) pipelines, respectively. For the single pulse pipeline, data are acquired in the form of a time, frequency and total intensity matrix. These are fed to the transient detection pipeline, HEIMDALL¹, which applies sliding boxcar filters of various widths and performs a threshold search. This produces candidate detections that are classified as FRBs if they meet the following

criteria:

$$\begin{aligned} \text{DM} &\geq 1.5 \times \text{DM}_{\text{Galaxy}} \\ \text{S/N} &\geq 8 \\ N_{\text{beams,adj}} &\leq 4 \\ \text{W} &\leq 262.14 \text{ ms} \\ N_{\text{events}}(t_{\text{obs}} - 2s \rightarrow t_{\text{obs}} + 2s) &\leq 5 \end{aligned} \quad (1)$$

where DM and $\text{DM}_{\text{Galaxy}}$ are the dispersion measures of the candidate and the Milky Way contribution along the line of sight, respectively. The latter is estimated using the NE2001 model (Cordes & Lazio 2002). S/N is the peak signal-to-noise ratio of the candidate, $N_{\text{beams,adj}}$ is the number of adjacent beams in which the candidate is detected and W is the width of the boxcar. The final criterion measures the number of candidates detected within a 4-second window centred on the time of occurrence of the pulse. If there are too many candidates in a time region around the candidate of interest, it is flagged as RFI. These criteria are followed by the T-pipeline, and for the purposes of keeping the processing to real-time, for the F-pipeline, we raise the detection threshold to $\text{S/N} \geq 10$ and only search for pulses with widths $\text{W} \leq 8.192$ ms. When a candidate meets these criteria, an alert email is issued and an astronomer evaluates a series of diagnostic plots to determine the validity of the candidate. If the candidate is deemed credible, multi-wavelength follow-up is triggered. Upon detection of a candidate matching the above criteria, 8-bit full-Stokes data are saved to disk for further offline processing.

3 FRB DISCOVERIES

The individual pulse profiles for the FRBs are shown in Fig 1 and Table 1 presents their measured and derived properties. The FRBs were detected in single beam of the Parkes multi-beam receiver. Each FRB has a positional uncertainty with a radius of $7.5'$. The inferred properties including redshift, energy, co-moving and luminosity distance are derived using the YMW16 model (Yao et al. 2017) of the electron density in the Milky Way. Our results are consistent within the uncertainties if we adopt the NE2001 model (Cordes & Lazio 2002) instead. To measure the scattering properties of the bursts, the procedure adopted in Champion et al. (2016) was applied. The resulting scattering time was scaled to a standard frequency of 1 GHz, using a spectral index of -4 . In the fitting process, we varied the assumed intrinsic width of the burst and find in all cases that the best fit is given by a burst duration that is solely determined by a combination of DM-smearing across the filterbank channels and interstellar scattering. Hence, due to the high DM of the FRBs reported here, all four FRBs are unresolved in width. We note that the estimated isotropic energies of the FRBs at source had an incorrect redshift correction in Caleb et al. (2016). The FRBs analysed at that time were mainly at redshifts $z < 1$, and the conclusions of the paper are unaffected. In this paper, three of the reported FRBs have $\text{DM} > 1500 \text{ pc cm}^{-3}$, for which cosmological effects become important. We follow Hogg (2000) and estimate the in-band intrinsic energies of the FRBs as:

$$E(J) = \frac{\mathcal{F}_{\text{obs}} \times BW \times 4\pi D_L^2 \times 10^{-29}}{(1+z)^{1+\alpha}} \quad (2)$$

where \mathcal{F}_{obs} is the observed fluence for FRBs in Jy ms, BW is the bandwidth at Parkes in Hz, D_L is the luminosity distance in meters, z is the inferred redshift of FRBs and α is the spectral index

¹ <https://sourceforge.net/projects/heimdall-astro/>

of the source. Note that the denominator incorporates both the k -correction for the spectral index and the time-dilation correction. Since we generally assume the spectral index to be flat and thus $\alpha = 0$, there is no k -correction in practice.

FRB 150610 was not detected in the F-pipeline. The reason for this was the final selection criterion described in Equation 1. At the time of observation, the number of events detected in a 4-second window did not make a distinction *by beam* and as such was overly harsh. In this case, one beam (beam 10) had a large number of RFI events in the time window, which resulted in all other (unrelated) beams being flagged. This criterion has since been corrected in the F-pipeline. FRB 150610 was discovered in the T-pipeline which makes less severe cuts to generated candidates. Since this burst was found in the offline processing, no prompt follow-up observations could be performed upon detection. The burst is slightly scattered but unresolved.² We determine the frequency dependence of the observed dispersion, $t_{\text{delay}} \propto \text{DM} \times \nu^{-\beta}$, to be $\beta = 2.000 \pm 0.008$, perfectly consistent with a cold-plasma law.

FRB 151206 fell *just* between search trials in the F pipeline, placing it slightly below the detection threshold. However the T-pipeline (which samples DM parameter space more completely) identified it soon after. As a result the full-Stokes data were not retained and no polarisation information is available. The burst is unresolved and slightly scattered. The limited signal-to-noise ratio prevents a fit for the DM index. The trigger was issued only 25 hours after the time of occurrence and eleven telescopes observed the Parkes position over the following days to months. Observations and results from each of these telescopes are described in §4.

FRB 151230 shows peak intensity near the centre of our observing band, similar to some of the events described in Spitler et al. (2016) for FRB 121102. The FRB is bright in the upper 200 MHz of the band and disappears at the lower frequencies in the band, below 1300 MHz. The burst is unresolved and shows scattering, possibly partly responsible for the non-detection at the lowest frequencies. We can determine the DM-index to be $\beta = 2.00 \pm 0.03$. This burst was discovered by the F-pipeline, an alert was raised, and a trigger was issued to telescopes after an hour of the detection. This burst was followed up by 12 telescopes ranging from radio to gamma-ray wavelengths.

FRB 160102 is the highest-DM FRB yet observed with $\text{DM} = 2596.1 \pm 0.3 \text{ pc cm}^{-3}$, and has an inferred luminosity distance of 17 Gpc, assuming the nominal redshift $z = 2.1$ from the models of Ioka (2003) and Inoue et al. (2014) for the observed DM excess. We find indications of scattering and determine the DM-index to $\beta = 2.000 \pm 0.007$. For this FRB, a trigger was issued approximately one hour after the event and this burst was followed up by 8 telescopes spanning radio to gamma-ray wavelengths.

4 FOLLOW-UP STUDIES

Follow-up observations of each FRB's field were carried out with four optical telescopes, nine radio telescopes, one high energy telescope and the ANTARES neutrino detector. Fig. 2 shows the summary of observations performed on each field. Imaging observations with radio and optical telescopes were performed in order to search for any variable or transient sources that might be associated with the FRBs. Radio follow-up also included searching for repeat pulses

from each FRB location. A complete record of all observations performed is included in Tables A1 to A4 in the Appendix.

4.1 Radio follow-up for repeat bursts

Follow-up observations were performed with the Parkes telescope using the Berkeley Parkes Swinburne Recorder (BPSR) observing setup (Keith et al. 2010) immediately after the discovery of each real-time FRB. The Sardinia radio telescope (SRT; Bolli et al. 2015) observed the FRB fields in single pulse search mode at a centre frequency of 1548 MHz with a bandwidth of 512 MHz. Observations were also performed by the Lovell and Effelsberg radio telescopes (Lovell 1985; Hachenberg et al. 1973) in L-Band (1.4 GHz) and single pulse searches were performed with PRESTO (Ransom et al. 2002) around the DM of the FRB. The UTMOST telescope (Bailes et al. 2017) also observed three of the FRB fields (all except FRB 150610). The UTMOST observations were performed at 843 MHz with a bandwidth of 31 MHz in fan beam mode with 352 fan beams covering $4^\circ \times 2.8^\circ$ (see Caleb et al. (2017) for the details of this observing mode). The details of the time spent on each FRB field are listed in Table 2. None of the observations showed repeated bursts from their respective FRB fields.

4.2 Radio interferometric follow-up for possible counterparts

Radio imaging observations were performed using the Australian Telescope Compact Array (ATCA) (Wilson et al. 2011), VLA, the Giant Metrewave Radio Telescope (GMRT) (Ananthkrishnan 1995) and the e-Merlin radio telescope (Garrington et al. 2004), spanning 4 to 8 GHz and 1 to 1.4 GHz. The details of the observations, data analysis and variability criteria are listed in Appendix B. Here we present the results of the follow-ups and the implications of the variability are discussed in §5.

FRB 151206: ATCA observed the field of FRB 151206 on 2015 December 9, 3 days after the burst. Visibilities were integrated for 3 hours yielding a radio map with an rms noise of $50 \mu\text{Jy/beam}$ at 5.5 GHz and $60 \mu\text{Jy/beam}$ at 7.5 GHz. The declination of the FRB field ($\delta = -04^\circ$) was not favourable for ATCA observations, therefore no subsequent observations were performed and no variability analysis was conducted on these data.

This field was observed for eight epochs with the VLA starting from 2015 December 8. The radio images reached an rms of $10 - 25 \mu\text{Jy/beam}$. Observations at epoch 3 were severely affected by RFI and hence excluded from the analysis. To form mosaic images, each of the 7 single pointings were stitched together for every epoch and were deconvolved using the CLEAN algorithm (Högbom 1974). Two significantly variable sources were detected in this field, details of which are listed in Table 4. Fig. 3(a) shows their light curves. No non-radio counterpart was identified for either of the sources.

Observations were performed with the GMRT on 2015 December 9. The field was observed for 4 hours and the map yielded an rms of $30 \mu\text{Jy/beam}$. No subsequent observations were performed and no variability analysis was conducted on these data.

The field was also observed with e-Merlin on 2015 December 7 and 8. Observations ran from 14:00–19:30 UTC on December 7 and 09:30–19:30 on December 8. A total of 1,945 overlapping fields were imaged and then combined using the AIPS task FLATN. The combined image covered a circular area of $10'$ diameter and has an rms of $34 \mu\text{Jy/beam}$ (beam size = $171 \times 31 \text{ mas}$, $\text{PA}=19.4^\circ$). At the declination of the source, snapshot imaging is quite challenging for e-Merlin, so the combined full sensitivity image from 1.5 runs was

² In the lowest subbands a second peak is visible, but statistical tests suggest that it is not significant and caused by noise fluctuations.

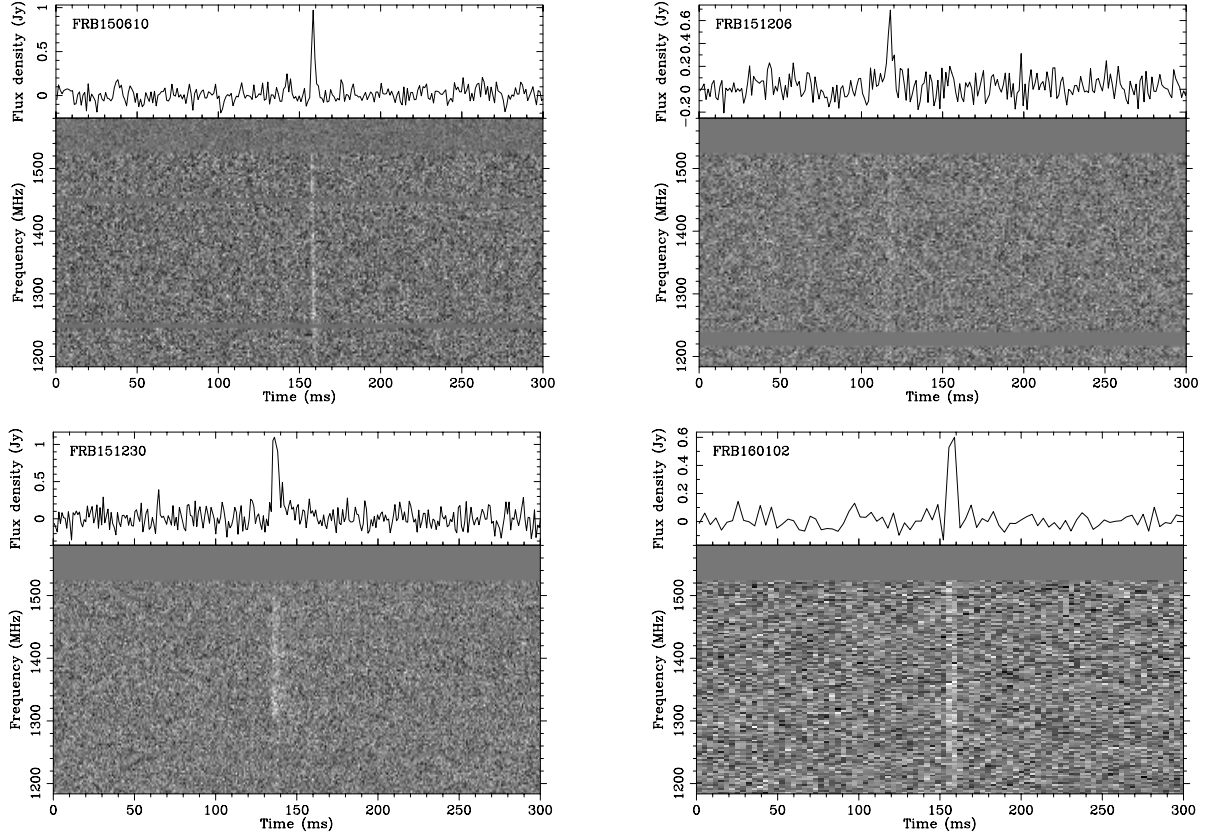


Figure 1. The pulse profiles of the four new FRBs de-dispersed to their best-fitting DM values: clock-wise from top left FRB 150610, FRB 151206, FRB 160102 and FRB 151230. The top panel shows the time series, frequency averaged to one channel and the bottom panel shows the spectrum of the pulse. The data have been time averaged to 1 ms, 0.6 ms, 0.8 ms and 0.5 ms per sample for FRB 150610, FRB 151206, FRB 160102 and FRB 151230 respectively. The flux density scale in the upper panel of individual pulses is derived from the radiometer equation. See table 1 for the dispersion smearing times within a single channel for each FRB.

Table 1. The observed and inferred (model-dependent) properties for FRBs 150610, 151206, 151230 and 160102. The model-dependent properties are derived using the YMW16 model (Yao et al. 2017) of the electron density in the Milky Way. For the cosmological parameters we use CosmoCalc (Wright 2006), adopting $H_0 = 69.9 \text{ km s}^{-1} \text{ Mpc}^{-1}$, $\Omega_M = 0.286$ and $\Omega_\Lambda = 0.714$. The error in the isotropic energy estimate is dominated by the error in the fluence.

| FRB YYMMDD | FRB 150610 | FRB 151206 | FRB 151230 | FRB 160102 |
|--|-------------------------|-------------------------|-------------------------|-------------------------|
| Measured Properties | | | | |
| Event time at 1.4 GHz UTC | 2015-06-10 05:26:59.396 | 2015-12-06 06:17:52.778 | 2015-12-30 16:15:46.525 | 2016-01-02 08:28:39.374 |
| Parke beam number | 02 | 03 | 04 | 13 |
| RA, DEC (J2000) | 10:44:26, -40:05:23 | 19:21:25, -04:07:54 | 09:40:50, -03:27:05 | 22:38:49, -30:10:50 |
| (ℓ , b) | 278.0°, 16.5° | 32.6°, -8.5° | 239.0°, 34.8° | 18.9°, -60.8° |
| Signal to noise ratio, (S/N) | 18 | 10 | 17 | 16 |
| Dispersion measure, DM (pc cm^{-3}) | 1593.9±0.6 | 1909.8±0.6 | 960.4±0.5 | 2596.1±0.3 |
| Scattering time at 1 GHz (ms) | 3.0±0.9 | 11±2 | 18±6 | 4±1 |
| Measured width, W50 (ms) | 2.0±1.0 | 3.0±0.6 | 4.4±0.5 | 3.4±0.8 |
| Instrumental dispersion smearing (ms) | 2.0 | 2.3 | 1.2 | 3.2 |
| Observed peak flux density, S_{peak} (Jy) | 0.7±0.2 | 0.30±0.04 | 0.42±0.03 | 0.5±0.1 |
| Measured fluence (Jy ms) | >1.3±0.7 | >0.9±0.2 | >1.9±0.3 | >1.8±0.5 |
| Model-dependent properties | | | | |
| DM_{Gal} (pc cm^{-3}) | ~122 | ~160 | ~38 | ~13 |
| Max. inferred z | 1.2 | 1.5 | 0.8 | 2.1 |
| Max. comoving distance (Gpc) | 3.9 | 4.3 | 2.7 | 5.5 |
| Max. luminosity distance (Gpc) | 8.6 | 10.6 | 4.8 | 17.2 |
| Max. isotropic energy (10^{33} J) | 1.8±1.0 | 1.7±0.4 | 1.0±0.2 | 7.0±2.0 |
| Average luminosity (10^{36} W) | 0.9±0.7 | 0.6±0.2 | 0.2±0.04 | 2.0±0.7 |

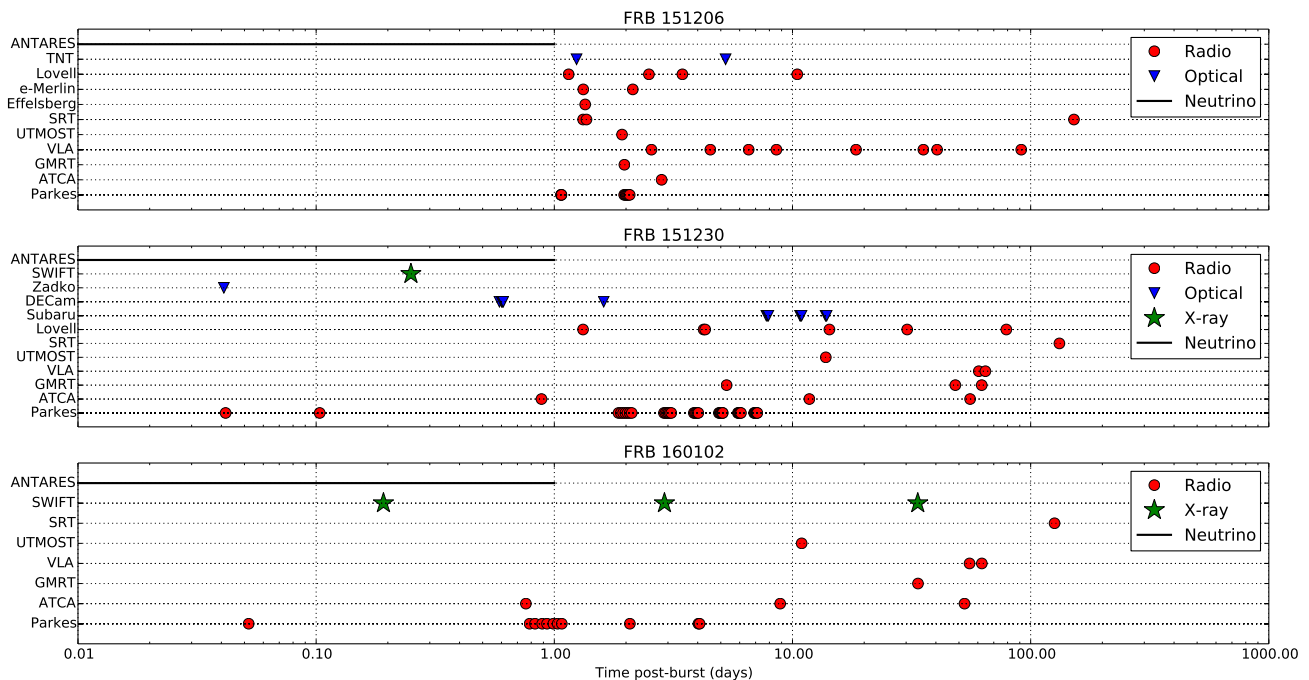


Figure 2. Multi-messenger follow-up campaign for FRBs 151206, 151230, 160102. The black line represents a part of the search for neutrino counterparts with ANTARES over the window $[T_0 - 1 \text{ day}; T_0 + 1 \text{ day}]$, where T_0 is the event time. No high energy follow-up was performed for FRB 151206 as it was Sun-constrained. Also, due to the delayed detection of FRB 150610 the multi-messenger follow-up was restricted to an ANTARES search alone.

Table 2. The time spent by the Parkes, SRT, Effelsberg, Lovell and UTMOST radio telescopes on the field of SUPERB FRBs to search for repeating pulses. None of the observations showed repeated bursts.

| FRB | Parkes $T_{\text{obs}}(\text{hrs})$ | SRT $T_{\text{obs}}(\text{hrs})$ | Effelsberg $T_{\text{obs}}(\text{hrs})$ | Lovell $T_{\text{obs}}(\text{hrs})$ | UTMOST $T_{\text{obs}}(\text{hrs})$ | Total (hrs) |
|------------|--|-------------------------------------|--|--|--|----------------|
| FRB 150610 | 10 | - | - | - | - | 10 |
| FRB 151206 | 3 | 9.3 | 3 | 3.3 | 3.75 | 22.3 |
| FRB 151230 | 36 | 2.9 | - | 8.5 | 7.5 | 54.9 |
| FRB 160102 | 9.2 | 2 | - | - | 4.7 | 15.9 |

searched for significant detections with SExtractor and nothing significant (> 6 -sigma) was found.

FRB 151230: ATCA was triggered ~ 1 day after the event and visibilities were recorded for 8 hours. Subsequent observations were performed on 2016 January 11 and 2016 February 24 for 9.5 and 4.5 hours, respectively. We performed a variability analysis of all compact sources at 5.5 GHz and 7.5 GHz. Following the criteria described in Appendix B, we conclude that there are no significant variable sources present in the field of FRB 151230.

Observations were performed using the VLA on 2016 February 29 and 2016 March 4 and images were produced at the center frequency of 5.9 GHz with an rms of $\sim 15 \mu\text{Jy}/\text{beam}$. All ATCA sources were detected. None of the compact sources were found to be significantly variable.

GMRT observations were performed on 2016 January 6, 2016 February 17 and 2016 March 3. The integration times of 4 hours yielded an rms of $\sim 30 \mu\text{Jy}/\text{beam}$ at 1.4 GHz. None of the sources showed any significant variability.

FRB 160102: ATCA observed the FRB 160102 field on 2016 January 3, 2016 January 11 and 2016 February 24. The best map yielded an rms of $\sim 40 \mu\text{Jy}/\text{beam}$ at 5.5 GHz and $\sim 50 \mu\text{Jy}/\text{beam}$ at 7.5 GHz. The search for sources was performed over an area of sky that is twice the region of the localisation error, i.e. a radius of

$15'$ because this FRB was detected in the outer beam of the Parkes telescope.

The final variability analysis was performed on 10 compact sources. Source 2238–3011 was found to vary significantly at 5.5 GHz but not at 7.5 GHz. We identify it to the quasar 2QZ J223831.1–301152 from the ‘‘Half a Million Quasar Survey’’ (Flesch 2015) at $z = 1.6$. This source is also present in the GALEX survey (Bianchi et al. 2011) (GALEX J223831.1–301152) and has a DSS (Eisenstein et al. 2011) optical counterpart. Table 4 and Figure 3(b) lists the details and light-curve of the source 2238–3011. The flux density of the source was observed to be rising at ATCA epochs at 5.5 GHz.

The VLA observations were performed on 2016 February 26 and 2016 March 4. Flux densities were derived from mosaics with the best rms being $\sim 10 \mu\text{Jy}/\text{beam}$. ATCA source 2238–3011 showed a low level variability with the fractional change (defined in Appendix B), $\Delta S \sim 20\%$ ($< 50\%$). None of the remaining sources were found to vary significantly at 5.9 GHz.

The field was also observed with the GMRT on 2016 February 6. The integration of 4 hours yielded an rms of $\sim 30 \mu\text{Jy}/\text{beam}$. This GMRT epoch was used to cross-check sources detected in the ATCA and VLA images and no variability analysis was performed on these data.

The results of the radio follow-up are summarised in Table 3.

4.3 Follow-up at non-radio frequencies

We have carried out optical and high energy follow-up and searched for neutrino counterparts to these four SUPERB FRBs. The results are presented in this section and the details of the observations and magnitude limits are listed in Appendix C.

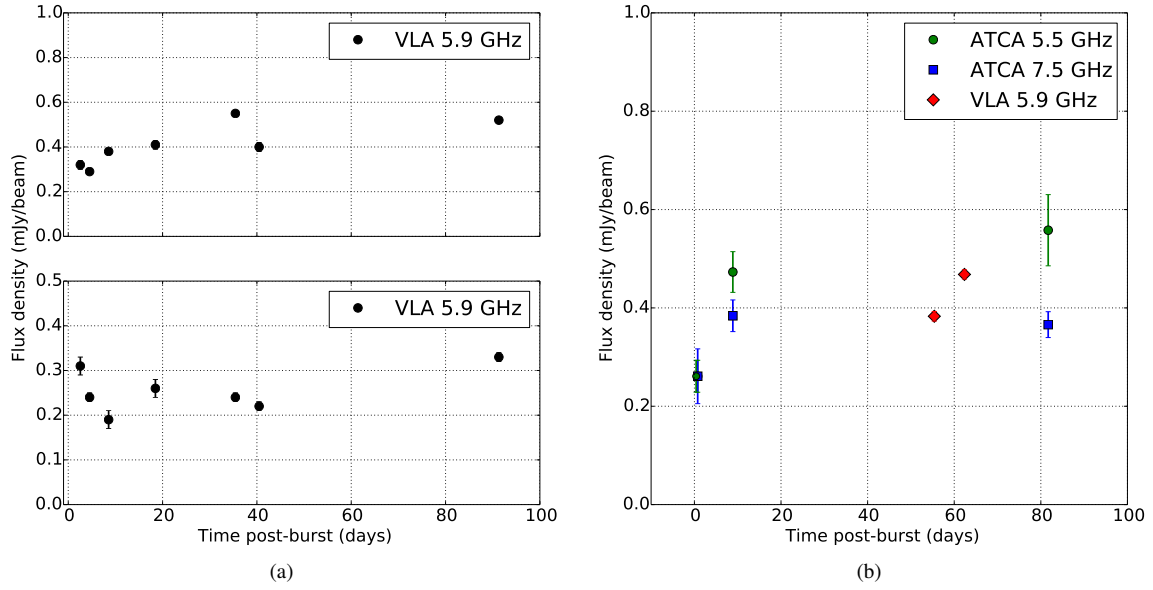


Figure 3. Left panel: The light-curves over 92 days of two sources in the field of FRB 151206 found to vary significantly in the VLA observations: 1921–0414 (top panel) and 1921–0412 (bottom panel). Right panel: The light curve of the significant variable source 2238–3011 in the field of FRB 160102. The fluxes and errors on fitting are derived from the task *IMFIT* in *miriad*. Note that the data have not been calibrated to the same absolute flux scale, and there may be systematic differences between different instruments. However, the data are self-consistent for variability analysis for each instrument.

Table 3. The results of the radio follow-up performed using the ATCA, VLA and GMRT on the fields of SUPERB FRBs. N_{total} denotes the total number of sources detected above 6-sigma and N_{analysis} are the number of sources used in the variability analysis. This excludes extended sources in the field of respective FRBs. N_{variable} denotes the number of significant variable sources detected in each field.

| Telescope | ATCA | | | VLA | | | GMRT | | | | | |
|--------------|--------------------|-----------------------|-----------------------|--------------------|-----------------------|-----------------------|--------------------|-----------------------|-----------------------|--------------------|-----------------------|-----------------------|
| | 5.5 GHz | | 7.5 GHz | 5.9 GHz | | | 1.4 GHz | | | | | |
| Centre freq. | N_{total} | N_{analysis} | N_{variable} | N_{total} | N_{analysis} | N_{variable} | N_{total} | N_{analysis} | N_{variable} | N_{total} | N_{analysis} | N_{variable} |
| FRB 151206 | 1 | - | - | 1 | - | - | 10 | 10 | 2 | 13 | - | - |
| FRB 151230 | 9 | 6 | 0 | 5 | 2 | 0 | 25 | 20 | 0 | 27 | 18 | 0 |
| FRB 160102 | 12 | 10 | 1 | 12 | 10 | 0 | 21 | 19 | 0 | 48 | - | - |

Table 4. Radio variable sources in the field of FRB 151206 and FRB 160102. The errors in RA and DEC are in arcseconds and are presented in brackets. Columns 4 and 5 list χ^2 and χ^2_{thresh} values. The χ^2_{thresh} values are upper-tail critical values of chi-square distribution with $N - 1$ degrees of freedom. Columns 6 and 7 list m_d , and ΔS values. These variability indices are defined in Appendix B.

| Name | RA | DEC | χ^2 | χ^2_{thresh} | m_d (%) | ΔS (%) |
|------------------|-------------------|--------------------|----------|--------------------------|--------------|-------------------|
| FRB 151206 field | | | | | | |
| VLA1921-0414 | 19:21:27.21 (0.2) | -04:14:55.67 (0.2) | 478.6 | 24.3 | 21.3 | 63.4 |
| VLA1921-0412 | 19:21:43.85 (0.2) | -04:12:17.43 (0.2) | 91.0 | 24.3 | 16.8 | 54.7 |
| FRB 160102 field | | | | | | |
| ATCA2238-3011 | 22:38:31.17 (0.2) | -30:11:51.38 (0.6) | 24.16 | 13.8 | 26.4 | 69.0 |

4.3.1 Thai National Telescope (FRB 151206)

The observations were performed with ULTRASPEC on the Thai National Telescope (TNT) on the night of 2015 December 7. Four optically variable sources were found in the field of FRB 151206. The change in magnitude Δmag provides a measurement of the

variability of a given source in the field, such that $\Delta\text{mag} > 0$ reflects a dimming source. The only source detected with a negative Δmag is also bright at infrared wavelengths, with $J = 9.38$, $H = 8.31$, $K = 7.93$ respectively from 2MASS (Skrutskie et al. 2006). Further photometric observations of the four variable sources were obtained using the 0.5-m robotic telescope ‘‘pt5m’’ (Hardy et al. 2015). In all

cases, the variability seen for these sources can be explained by stellar variability, either eclipsing, ellipsoidal or stochastic (accretion, flaring etc).

4.3.2 Subaru Telescope (FRB 151230)

We performed follow-up imaging observations of the field of FRB 151230 in the g -, r -, i -bands on 2016 January 7, 10 and 13, with Subaru/Hyper Suprime-Cam that covers a 1.5 deg diameter field-of-view. The images taken on January 13 were used as the reference images and were subtracted from the images of January 7 and 10 using the HSC pipeline (Bosch et al. 2017). Ninety-seven variable source candidates with either positive or negative flux difference were detected in the error circle of FRB 151230 on the differential images. These candidates were examined by eye, and approximately half of them appear to be real objects while the other half are artefacts by subtraction failure. Most of the real variable sources are likely to be either Galactic variable stars (point sources without host galaxy) or AGNs (variable sources located at centres of galaxies). There are three objects associated with galaxies and offset from galaxy centres, which are most likely supernovae. This number is consistent with those detected outside the FRB error region considering the area difference, and also consistent with a theoretically predicted number of supernovae with the depth and cadence of our observations (Niino et al. 2014). No object shows evidence for an association with the FRB, although we cannot exclude the possibility that one of them is associated. The nature of the variable objects will be investigated and discussed in detail in a forthcoming paper (Tominaga et al. in prep).

4.3.3 DECam (FRB 151230)

We obtained DECam u - g - r - i dithered images centred on the coordinates of FRB 151230, with observations taken approximately 14 hours after the detection at Parkes. The field was also re-observed with the g filter ~ 39 hours after the FRB detection. We searched these g -band images for transient sources (>10 -sigma significance) between the two consecutive nights, within the localisation error region of $15'$, using *Mary* pipeline (Andreoni et al., under review). We detected 5 variable sources and 4 of them were cataloged³ as small bodies, i.e. Main-belt asteroids. A fifth object was detected at a magnitude $g = 22.51 \pm 0.08$ on 2016 January 1, which had not been detected on the previous night, 2015 December 31 ($g < 23.37$ at 5-sigma confidence). This transient is located at RA=9:40:56.34, DEC=-3:27:38.29 (J2000) and is not present in the NASA/JPL small body catalog but is most likely to be an asteroid unrelated to FRB. However, it is not detected in the u - g - r - i images taken on 2015 December 31. All other transient events were rejected as bonafide transients due to poor local subtraction and bad pixels after a visual inspection of the residuals.

We have also compared the radio sources detected in the GMRT and ATCA images with the DECam images to look for optical counterparts; more details are given in Appendix C.

4.3.4 The Zadko Telescope (FRB 151230)

On 2015 December 30, the Zadko telescope was shadowing the Parkes telescope at the time of the discovery of FRB 151230. However, due to technical difficulties, the first science images were taken

at 18:03:20.6 UTC, i.e. ~ 1 hour after the FRB event. Following this initial imaging, a series of 19 images of 5 tiles each were obtained during about 2 hrs through to the end of the night. Each image had an exposure time of 60 seconds in the r -band. The localisation error region ($15'$) around FRB 151230 is completely covered by the central image of the tiles and partly contained ($\sim 33\%$) in the peripheral images.

We analysed the individual images to search for new optical or variable sources in the field of FRB 151230. We particularly focused on the central image of the tile that fully covers the error radius around the FRB position. We found no convincing new or variable optical sources.

4.3.5 High energy follow-up (FRB 151230, FRB 160102)

We acquired follow-up observations with *Swift* on FRB 151230 burst on 2015 December 30 at 23:14:45 UTC, about 7 hours after the FRB for a duration of 2.05 ks. No sources were detected above a 2.5-sigma limit in the X-ray image. The data were analysed using the tools available at the *Swift* website (Evans et al. 2007, 2009) on an observation-by-observation basis. Count rates were converted to X-ray flux assuming a GRB-like spectral index of -2.0 and Galactic HI column density estimates from the HEASoft tool “nH”.

We acquired 3 epochs on the field of FRB 160102 with the *Swift* XRT of durations 3.5 ks, 3.3 ks, and 1.8 ks, respectively. No sources were detected above a 2.5-sigma limit in any of the images. We did not trigger *Swift* for FRB 150610 (due to the delay in its detection), nor FRB 151206 (as it was Sun constrained for 31 days after the FRB).

No *Swift*-BAT REALTIME triggers were issued for short duration gamma-ray transients during the follow-up observations for each FRB field.

4.3.6 ANTARES follow-up (all FRBs)

Multi-messenger observations with high-energy neutrino telescopes can help to constrain the FRB origin and offer a unique way to address the nature of the accelerated particles in FRBs. The ANTARES telescope (Ageron et al. 2011) is a deep-sea Cherenkov neutrino detector, located 40 km off Toulon, France, in the Mediterranean Sea and dedicated to the observation of neutrinos with $E_\nu \gtrsim 100$ GeV. ANTARES aims primarily at the detection of neutrino-produced muons that induce Cherenkov light in the detector. Therefore, by design, ANTARES mainly observes the Southern sky (2π steradian at any time) with a high duty cycle. Searches for neutrino signals from the four detected FRBs have been performed within two different time windows around the respective FRB trigger time, T_0 , within a 2° radius region of interest (ROI) around the FRB position (3-sigma ANTARES point spread function for the online track reconstruction method). The first time window $\Delta T_1 = [T_0 - 500 \text{ s}; T_0 + 500 \text{ s}]$ is short and was defined for the case where FRBs are associated with short transient events, e.g. short Gamma-Ray Bursts (Baret et al. 2011). A longer time window $\Delta T_2 = [T_0 - 1 \text{ day}; T_0 + 1 \text{ day}]$ is then used to take into account longer delays between the neutrino and the radio emission. The number of atmospheric background events within the ROI is directly estimated from the data measured in the visible Southern sky using a time window $\Delta T_{\text{back}} = [T_0 - 12 \text{ hr}; T_0 + 12 \text{ hr}]$. The stability of the counting rates has been verified by looking at the event rates detected in time slices of 2 hours within ΔT_{back} . Within ΔT_1 and ΔT_2 , no neutrino events were found in correlation with FRB 150610, FRB 151206, FRB 151230 or FRB 160102.

³ NASA/JPL SB identification system: ssd.jpl.nasa.gov

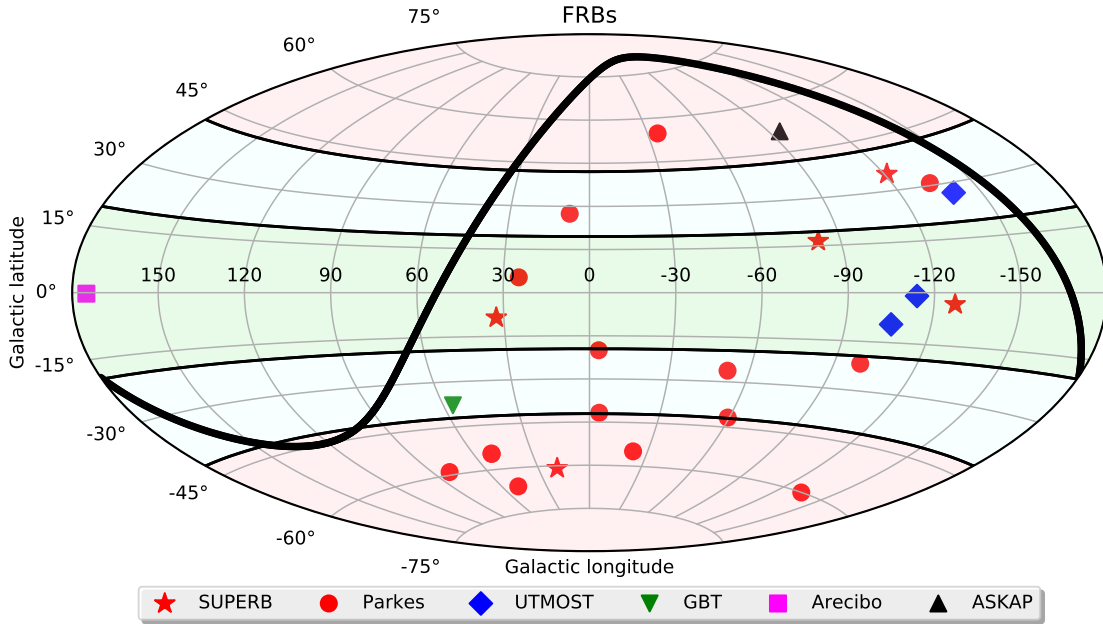


Figure 4. An Aitoff projection of the sky distribution of all published FRBs. The shaded regions show the three Galactic latitude bins in Table 5. The bold black line shows the horizon limit of the Parkes radio telescope.

Table 5. Time on sky in the three latitude bins for recent surveys conducted at the Parkes telescope: the High Time Resolution Universe survey (HTRU; [Keith et al. 2010](#)), observations of rotating radio transients, FRB follow-up, the SUPERB survey, and observations of young pulsars for *Fermi* timing. All surveys made, or make, use of the multi-beam receiver and have equivalent field of view and sensitivity limits. The FRB sky rates for respective latitude bins are quoted with 95% confidence.

| Galactic latitude $ b $ (deg) | HTRU medlat (hrs) | HTRU hilat (hrs) | RRAT search (hrs) | FRB follow-up (hrs) | SUPERB (hrs) | Fermi timing (hrs) | Misc time (hrs) | Total time (hrs) | N_{FRBs} | R_{FRB} FRBs sky $^{-1}$ day $^{-1}$ |
|-------------------------------------|-------------------------|------------------------|-------------------------|---------------------------|-----------------|--------------------------|-----------------------|------------------------|-------------------|--|
| $ b \leq 19.5^\circ$ | 1157 | 402 | 483 | 0 | 700 | 281 | 0 | 3024 | 4 | $2.4^{+3.1}_{-1.5} \times 10^3$ |
| $19.5^\circ < b < 42^\circ$ | 0 | 942 | 28 | 50 | 1115 | 10 | 100 | 2245 | 6 | $4.8^{+4.6}_{-2.7} \times 10^3$ |
| $42^\circ \leq b \leq 90^\circ$ | 0 | 982 | 39 | 60 | 907 | 9 | 90 | 2088 | 9 | $7.8^{+5.8}_{-3.7} \times 10^3$ |

5 RESULTS AND DISCUSSION

5.1 Cosmological implications of high DM FRBs

Assuming FRBs are extragalactic, the DM may be divided into contributions along the line-of-sight from the ISM in the Milky Way (DM_{Galaxy}), the Intergalactic Medium (DM_{IGM}), a host galaxy (DM_{host}) and the circum-burst medium (DM_{source}):

$$DM_{\text{FRB}} = DM_{\text{Galaxy}} + DM_{\text{IGM}} + DM_{\text{host}} + DM_{\text{source}}. \quad (3)$$

For all the FRBs reported here, the DM_{Galaxy} contribution is minor ($< 10\%$ of the total observed DM). It is currently difficult to disentangle the DM contributions of the remaining DM terms for these bursts. [Xu & Han \(2015\)](#) showed the DM_{host} to peak in the range of 30 to 300 pc cm^{-3} for different inclination angles of a spiral galaxy and average DM_{host} to be 45 pc cm^{-3} and 37 pc cm^{-3} for a dwarf and an elliptical galaxy respectively. In such cases, the remaining DM is expected to arise from the IGM if the sources are cosmological in nature.

If the DM of our FRBs is indeed dominated by the IGM contribution, then we are potentially probing the IGM at redshifts beyond $z \gtrsim 2$. If we can find FRBs with $DM \gtrsim 3000 \text{ pc cm}^{-3}$, we could begin to probe the era in which the second helium reionisation in

the Universe occurred ([Fialkov & Loeb 2016](#)), which is important for determining the total optical depth to reionisation of the Cosmic Microwave Background (CMB), τ_{CMB} . We note that we discovered FRB 160102 soon after our pipelines were modified to allow for DM searches above 2000 pc cm^{-3} (the current upper limit is 10,000 pc cm^{-3}). Even in the absence of scattering being a dominant factor higher sensitivity instruments will likely be needed to probe such high redshifts.

5.2 FRB latitude dependence revisited

With an ever increasing sample of FRBs detected with the BPSR backend it is worthwhile to revisit the Galactic latitude dependence in FRB detectability first examined in [Petroff et al. \(2014\)](#). Table 5 summarises the data from SUPERB, as well as several other projects using BPSR that have each observed the sky with essentially the same sensitivity to FRBs resulting in the total of 19 bursts. We consider three regions on the sky, delineated in Galactic latitude as follows: $|b| \leq 19.5^\circ$, $19.5^\circ < |b| < 42^\circ$, and $42^\circ \leq |b|$. The time on sky in each of these regions and the updated FRB rate at the 95% confidence level are presented in the table. Fig. 4 shows these FRBs on an Aitoff projection in the Galactic coordinate frame. For

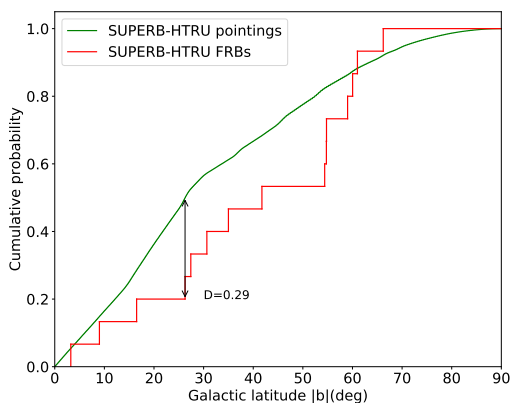


Figure 5. The observed cumulative distribution of Galactic latitude $|b|$ of FRBs detected in HTRU and SUPERB and the expected integration-time-weighted cumulative distribution of Galactic latitude $|b|$ for isotropically distributed FRBs. A K-S test indicates that the FRB distribution does not deviate significantly from isotropy.

the studies considered here Parkes has spent $\sim 42\%$ of the total time in the lowest Galactic latitude region (this is mostly driven by pulsar searches and/or continued monitoring studies). Despite this only 4 of the 19 bursts have been found in this range. At the highest latitudes 9 FRBs have been detected in $\sim 40\%$ of the total time. We performed a Kolmogorov-Smirnov test (K-S) between the expected cumulative distribution of $|b|$ for isotropically distributed FRBs based on the integration-time-weighted Galactic latitudes of the combined HTRU-SUPERB survey pointings, and the observed cumulative distribution of the 15 FRBs (see Fig 5). We obtain the KS statistic D and p values of 0.29, 0.10 respectively, and conclude that departure from isotropy is not significant. Thus any disparity in the FRB rate with Galactic latitude has low significance ($< 2\sigma$) in our now larger sample of 15 FRBs. If such a disparity exists, it could be explained by diffractive scintillation boosting at high Galactic latitudes as discussed in Macquart & Johnston (2015).

5.3 FRB populations and distributions

Sources with constant space density in a Euclidean Universe yield an integral source counts, N , as a function of fluence, \mathcal{F} , the so-called “logN-log \mathcal{F} ”-relation, with a slope of $-3/2$. The relation flattens in Λ CDM cosmologies, depending on the redshift distribution of the sources being probed, and depends to some extent on the luminosity function of the sources, and observational factors like the effects that DM smearing have on the S/N of events (Caleb et al. 2016; Vedantham et al. 2016; CHIME Scientific Collaboration et al. 2017).

In Fig. 6(a), we present the FRB source count distribution as a function of fluence, for FRBs found with the BPSR instrument at Parkes. The sample consists of 10 FRBs found in the HTRU survey (Thornton et al. 2013; Champion et al. 2016); Petroff et al (in prep), 5 FRBs found with SUPERB (Keane et al. 2016, FRB 150418) and this paper, and 4 FRBs found at Parkes with the same instrumentation and search technique (Ravi et al. 2015, 2016; Petroff et al. 2015b, 2017).

We note the following caveats about the logN-log \mathcal{F} distribution. Firstly, the fluences are lower limits, as most of the FRBs are poorly localised within the Parkes beam pattern. Secondly, all FRB surveys are incomplete below some fluence, due to the effects of DM smearing, scattering and the underlying width distribution of the events (see §5.4 and Fig. 7). Although both these affect the shape

of logN-log \mathcal{F} , simulations performed by Caleb et al. (2016) show that the slope of the relation is mainly set by cosmological effects. They found $\alpha = -0.9 \pm 0.3$ for the 9 HTRU FRBs.

We measure a slope of the integral source counts using the maximum likelihood method (Crawford et al. 1970) and obtain $\alpha = -2.2^{+0.6}_{-1.2}$ for FRBs above a fluence limit of 2 Jy ms as shown in Fig 6(b). This is consistent with the source count slope for Parkes FRBs found by Macquart & Ekers (2017), who find $\alpha = -2.6^{+0.7}_{-1.3}$. The large uncertainty in α is due to the small sample size. Similarly to Macquart & Ekers (2017), we are unable to rule out that the source counts are not Euclidean ($\alpha = -3/2$).

5.4 Parkes sky rates

With the increased number of FRBs we update the all-sky rate estimates for Parkes. The all-sky lower limit on the rate is $4.7^{+2.1}_{-1.7} \times 10^3$ FRBs/(4 π sr)/day. This is based on the observed rate of 19 events in 306 days of observing with BPSR, assuming the events occur within the full-width-half-power field-of-view of the receiver, and extrapolating this to the entire sky. The quoted uncertainties are 95% Poisson uncertainties (Gehrels 1986). Additionally we update the fluence complete rate, which is a more useful quantity when scaling FRB rates to other telescopes and/or frequencies. Figure 7 shows the observed peak flux density and observed widths of the FRB population, with Parkes sensitivity and completeness regions highlighted. Following Keane & Petroff (2015) and considering those FRBs in the fluence complete region we estimate a rate above ~ 2 Jy ms of $1.7^{+1.5}_{-0.9} \times 10^3$ FRBs/(4 π sr)/day.

5.5 Variable and transient source densities in the field of FRBs

We essentially performed a targeted survey to search for significantly variable and transient radio sources in the three of our FRB fields. We covered ~ 0.15 deg 2 of sky for all fields with VLA at a sensitivity of ~ 100 μ Jy and ~ 0.3 deg 2 of sky for all fields with ATCA at a sensitivity of ~ 300 μ Jy from 4 GHz to 8 GHz. We detected two sources in the VLA images of the field of FRB 151206 and one source in the ATCA images of the field of FRB 160102 to vary significantly.

However, no radio transients were detected. The significant variable source surface density for our survey is $\rho_v = 10^{+9.7}_{-5.4}$ deg $^{-2}$ (1-sigma Poisson error). The Poisson uncertainties are calculated following Gehrels (1986). The upper limits on the transient source density for zero detections at 95% confidence is given by $\rho_t < 0.56$ deg $^{-2}$ above the flux limit of 100 μ Jy. (Fig 8(b)).

Bell et al. (2015) performed a search for variable sources in ~ 0.3 deg 2 with comparable flux limits and at similar frequencies as our search. They reported $\rho_v = 3.3^{+7.5}_{-2.7}$ deg $^{-2}$ (1-sigma Poisson error) for significant variable sources. We also compared our ρ_v with Becker et al. (2010) and Mooley et al. (2016). The results are presented in Fig 8(a). The flux density limit (S_{\min}) and ρ_v for Mooley et al. (2016) were scaled to 5.5 GHz from 3 GHz using the relation $S_{\min} \propto \nu^\alpha$ and $\rho_v \propto S_{\min}^{-1.5}$ where ν is the frequency and α is the spectral index (which is assumed to be -0.7). We find that the surface density of significant variable sources is consistent within the uncertainty estimates with surveys done in the past in non-FRB fields. Consequently, we find no strong evidence that the FRBs reported here are associated with the highly variable sources in the fields, subject to the caveats that somewhat different variability

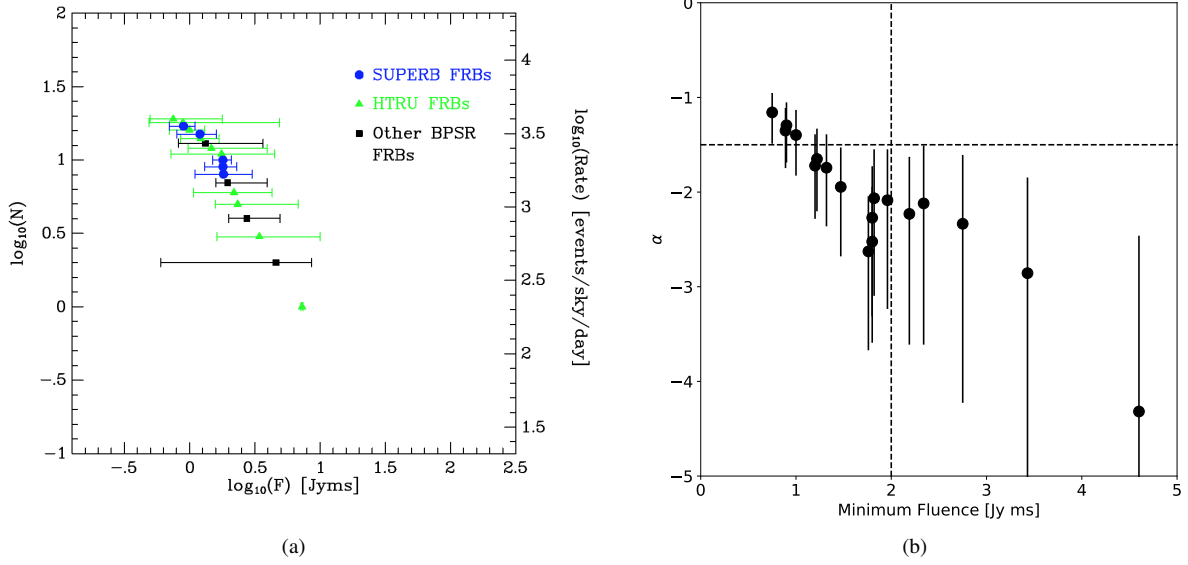


Figure 6. Left panel: The source count distribution of Parkes FRBs. The sky rate is indicated on the right, normalised to rate of 1.7×10^3 FRBs $\text{sky}^{-1} \text{day}^{-1}$ for $\mathcal{F} > 2$ Jy ms (see §5.4). Right panel: The slope α of the integral source counts obtained using the maximum likelihood method (Crawford et al. 1970). We obtain a slope of $\alpha = -2.2^{+0.6}_{-1.2}$ for FRBs above a fluence completeness limit of 2 Jy ms in our updated sample of 19 FRBs. The vertical dashed line indicates the fluence completeness limit and the horizontal dashed line indicates $\alpha = -3/2$, the slope expected for constant space density sources distributed in a Euclidean Universe.

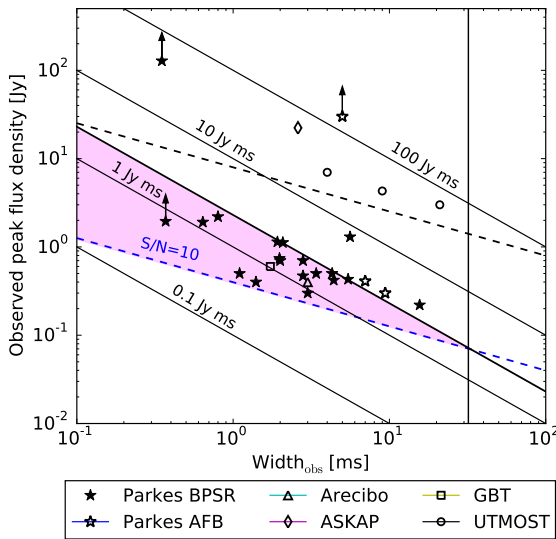


Figure 7. The observed peak flux density and observed width for all known FRBs. The sensitivity limits and fluence completeness region for BPSR Parkes events are indicated. These do not apply to other events which are shown for reference only.

search criteria, different frequencies and different sensitivity limits were used in the comparison surveys.

The probability of detecting N variable sources in an area A is given by:

$$P(N) = \int_0^{\infty} P(N | \sigma) P(\sigma) d\sigma \quad (4)$$

where, σ is the variable source density, $P(\sigma)$ is the prior probability for that variable, normalised such that $\int_0^{\infty} P(\sigma) d\sigma = 1$. We calculate the prior probability using Bell et al. (2015) as our control

survey, which is given by:

$$P(\sigma) = C \sigma^{N_0} e^{-\sigma A_0} \quad (5)$$

where C is the normalisation constant, N_0 and A_0 are the number of highly variable source and the area covered in the control survey. We use results from our VLA observations of FRB fields to compare with the control survey because of their comparable sensitivities and found that the probability of detecting two highly variable sources in a $\sim 0.15 \text{ deg}^2$ area of sky is 14.8%. Currently with the available data, we lack sufficient information to conclusively associate any of these variable sources with FRB 151206 or FRB 160102. However, the detection of a known variable quasar in the field of FRB 160102, the presence of variable AGN in the field of FRB 150418 (Johnston et al. 2017), FRB 131104 (Shannon & Ravi 2016) and the persistent variable radio source in the field of FRB 121102 (Chatterjee et al. 2017) hint that FRBs might be related to AGN activity in the host galaxy, however in the absence of a large FRB population and their localisation, this remains speculative.

6 SUMMARY AND CONCLUSIONS

We report the discoveries of four new FRBs in the SUPERB survey being conducted with the Parkes radio telescope: FRB 150610, 151206, 151230 and 160201. We have performed multi-messenger follow-up of these using 2, 11, 12 and 8 telescopes respectively. No repeating radio pulses were detected in 103.1 hrs of radio follow-up. We continue to follow all SUPERB and bright HTRU FRBs in our ongoing SUPERB observations.

A comparison of the repeating FRB with the published non-repeating FRBs has been performed by Palaniswamy & Zhang (2017), who present evidence that there are two distinct populations of FRBs – repeating and non-repeating – based on the distribution of pulse fluences and the amount of followup time for each

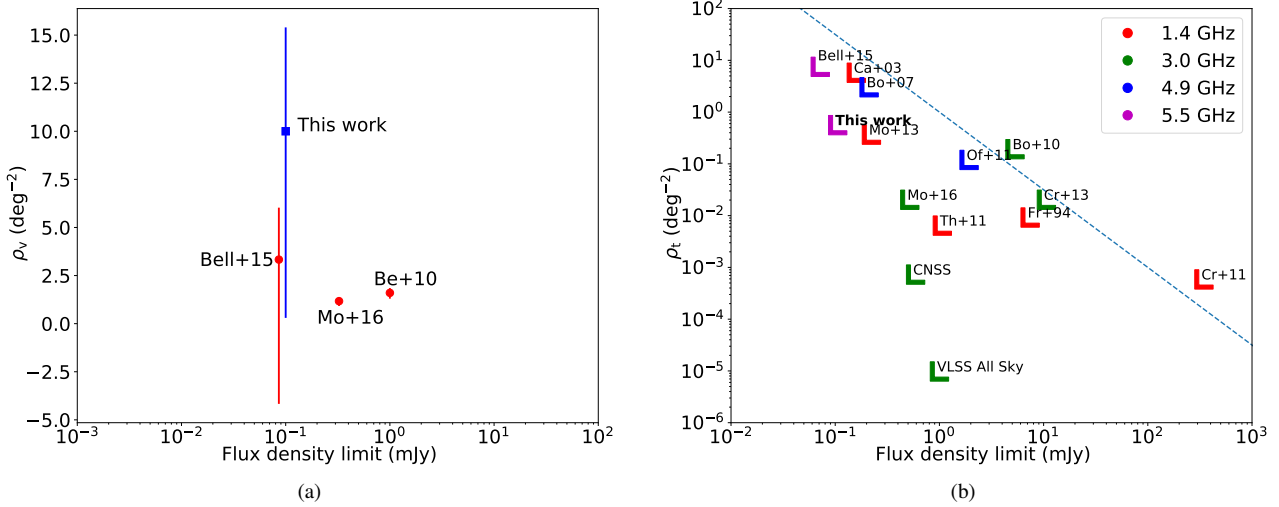


Figure 8. Left panel: The density of significantly variable radio sources as a function of flux density in surveys made at ~ 5 GHz and 3 GHz by Bell et al. (2015), this work, Becker et al. (2010) and Mooley et al. (2016). The density of significantly variable sources is consistent within a 1-sigma Poisson error for surveys done in the past. Right panel: The density of transient radio sources in surveys conducted at 1.4 GHz (Carilli et al. 2003; Mooley et al. 2013; Thyagarajan et al. 2011; Frail et al. 1994; Croft et al. 2011), 3 GHz (Bower et al. 2010; Croft et al. 2013; Mooley et al. 2016, CNSS pilot, CNSS, VLSS), 4.9 GHz (Bower et al. 2007; Ofek et al. 2011), and 5.5 GHz (This work, Bell et al. (2015)) as a function of flux density. The dashed blue line shows $\rho_t \propto S^{-3/2}$. This is the relation for a Euclidean population.

Table 6. Comparison of the properties of the FRBs detected in SUPERB and the repeating FRB 121102. SUPERB FRBs are unresolved in time and show scattering unlike the repeater.

| Property | FRB 121102 | SUPERB FRBs |
|----------------------------------|------------|----------------|
| ~ 100 MHz spectral features | Yes | 1 of 5 sources |
| time resolved | Yes | No |
| range of spectral index | -15 to +10 | ~ 0 |
| scattering | No | Yes |
| width | 3 – 9 ms | < 0.8 – 4 ms |

source. The FRBs reported here differ from FRB121102 (the repeating FRB) in a number of ways, as shown in Table 6. The pulses from the repeater are time resolved and their pulse widths vary from 3–9 ms whereas the SUPERB FRBs are unresolved (in time): the width is instead dominated by the effects of DM smearing and scattering. This appears to provide further support for the two source population conclusion of Palaniswamy & Zhang (2017).

With our larger sample of FRBs detected at Parkes, we have revisited the FRB event rate and derived an updated all sky FRB rate of $1.7^{+1.5}_{-0.9} \times 10^3$ FRBs/(4 π sr)/day above a fluence of ~ 2 Jy ms. We have also computed the volumetric rate of FRBs for the 19 FRB sample using the fluence complete rate as our basis. We get volumetric rates in the range 2000 to 7000 Gpc $^{-3}$ yr $^{-1}$ out to a redshift of $z \sim 1$. This is consistent with volumetric rates for a range of transients (e.g. low luminosity long GRBs, short GRBs, NS-NS mergers, and supernovae (CC, Type Ia, etc)) (Kulkarni et al. 2014; Totani 2013).

Our follow-up campaign of the reported FRBs yielded no multi-wavelength or multi-messenger counterparts and we have placed upper limits on their detection. We have also concluded that variability in the optical/radio images alone does not provide a reliable association with the FRBs. We encourage wide-field and simultaneous multi-wavelength observations of FRBs. In future, the

detection of FRBs with an interferometer would be able to provide a robust host galaxy association.

ACKNOWLEDGEMENTS

The Parkes radio telescope and the Australia Telescope Compact Array are part of the Australia Telescope National Facility which is funded by the Commonwealth of Australia for operation as a National Facility managed by CSIRO. Parts of this research were conducted by the Australian Research Council Centre of Excellence for All-sky Astrophysics (CAASTRO), through project number CE110001020. The GMRT is run by the National Centre for Radio Astrophysics of the Tata Institute of Fundamental Research. VLA is run by the National Radio Astronomy Observatory (NRAO). NRAO is a facility of the National Science Foundation operated under cooperative agreement by Associated Universities, Inc. This work was performed on the gSTAR national facility at Swinburne University of Technology. gSTAR is funded by Swinburne and the Australian Government’s Education Investment Fund. This work is also based on data collected at Subaru Telescope, which is operated by the National Astronomical Observatory of Japan. We thank the LSST Project for making their code available as free software at <http://dm.lsstcorp.org>. Funding from the European Research Council under the European Union’s Seventh Framework Programme (FP/2007-2013) / ERC Grant Agreement n. 617199 (EP). Access to the Lovell Telescope is supported through an STFC consolidated grant. The 100-m telescope in Effelsberg is operation by the Max-Planck-Institut für Radioastronomie with funds of the Max-Planck Society. The Sardinia Radio Telescope (SRT) is funded by the Department of University and Research (MIUR), the Italian Space Agency (ASI), and the Autonomous Region of Sardinia (RAS) and is operated as National Facility by the National Institute for Astrophysics (INAF). TB and RWW are grateful to the STFC for financial support (grant reference ST/P000541/1). Research support to IA is provided by the Australian Astronomical Observatory. The

ANTARES authors acknowledge the financial support of the funding agencies: Centre National de la Recherche Scientifique (CNRS), Commissariat à l'énergie atomique et aux énergies alternatives (CEA), Commission Européenne (FEDER fund and Marie Curie Program), Institut Universitaire de France (IUF), IdEx program and UnivEarthS Labex program at Sorbonne Paris Cité (ANR-10-LABX-0023 and ANR-11-IDEX-0005-02), Labex OCEVU (ANR-11-LABX-0060) and the A*MIDEX project (ANR-11-IDEX-0001-02), Région Île-de-France (DIM-ACAV), Région Alsace (contrat CPER), Région Provence-Alpes-Côte d'Azur, Département du Var and Ville de La Seyne-sur-Mer, France; Bundesministerium für Bildung und Forschung (BMBF), Germany; Istituto Nazionale di Fisica Nucleare (INFN), Italy; Stichting voor Fundamenteel Onderzoek der Materie (FOM), Nederlandse organisatie voor Wetenschappelijk Onderzoek (NWO), the Netherlands; Council of the President of the Russian Federation for young scientists and leading scientific schools supporting grants, Russia; National Authority for Scientific Research (ANCS), Romania; Ministerio de Economía y Competitividad (MINECO): Plan Estatal de Investigación (refs. FPA2015-65150-C3-1-P, -2-P and -3-P, (MINECO/FEDER)), Severo Ochoa Centre of Excellence and MultiDark Consolider (MINECO), and Prometeo and Grisolíá programs (Generalitat Valenciana), Spain; Ministry of Higher Education, Scientific Research and Professional Training, Morocco. We also acknowledge the technical support of Ifremer, AIM and Foselev Marine for the sea operation and the CC-IN2P3 for the computing facilities. This work made use of data supplied by the UK Swift Science Data Centre at the University of Leicester. This research has made use of data, software and/or web tools obtained from the High Energy Astrophysics Science Archive Research Center (HEASARC), a service of the Astrophysics Science Division at NASA/GSFC and of the Smithsonian Astrophysical Observatory's High Energy Astrophysics Division. This work is based in part on data collected at Subaru Telescope, which is operated by the National Astronomical Observatory of Japan. This paper makes use of software developed for the Large Synoptic Survey Telescope. We thank the LSST Project for making their code available as free software at <http://dm.lsstcorp.org>. RPE/MK gratefully acknowledges support from ERC Synergy Grant "BlackHoleCam" Grant Agreement Number 610058

SB would like to thank Tara Murphy, Martin Bell, Paul Hancock, Keith Bannister, Chris Blake and Bing Zhang for useful discussions.

REFERENCES

- Adrian-Martínez S., et al., 2016, preprint, ([arXiv:1608.08840](https://arxiv.org/abs/1608.08840))
- Ageron M., et al., 2011, *Nuclear Instruments and Methods in Physics Research A*, **656**, 11
- Alard C., 2000, *A&AS*, **144**, 363
- Alard C., Lupton R. H., 1998, *ApJ*, **503**, 325
- Ananthakrishnan S., 1995, *Journal of Astrophysics and Astronomy Supplement*, **16**, 427
- Axelrod T., Kantor J., Lupton R. H., Pierfederici F., 2010, in *Software and Cyberinfrastructure for Astronomy*. p. 774015, [doi:10.1117/12.857297](https://doi.org/10.1117/12.857297)
- Bailes M., et al., 2017, preprint, ([arXiv:1708.09619](https://arxiv.org/abs/1708.09619))
- Bannister K., et al., 2017, preprint, ([arXiv:1705.07581](https://arxiv.org/abs/1705.07581))
- Baret B., et al., 2011, *Astroparticle Physics*, **35**, 1
- Becker R. H., Helfand D. J., White R. L., Proctor D. D., 2010, *The Astrophysical Journal*, **140**, 157
- Bell M. E., Huynh M. T., Hancock P., Murphy T., Gaensler B. M., Burlon D., Trott C., Bannister K., 2015, *MNRAS*, **450**, 4221
- Bianchi L., Herald J., Efremova B., Girardi L., Zobot A., Marigo P., Conti A., Shiao B., 2011, *Ap&SS*, **335**, 161
- Bolli P., et al., 2015, *Journal of Astronomical Instrumentation*, **4**, 1550008
- Bosch J., et al., 2017, preprint, ([arXiv:1705.06766](https://arxiv.org/abs/1705.06766))
- Bower G. C., Saul D., Bloom J. S., Bolatto A., Filippenko A. V., Foley R. J., Perley D., 2007, *ApJ*, **666**, 346
- Bower G. C., et al., 2010, *ApJ*, **725**, 1792
- Burke-Spolaor S., Bannister K. W., 2014, *ApJ*, **792**, 19
- CHIME Scientific Collaboration et al., 2017, preprint, ([arXiv:1702.08040](https://arxiv.org/abs/1702.08040))
- Caleb M., Flynn C., Bailes M., Barr E. D., Hunstead R. W., Keane E. F., Ravi V., van Straten W., 2016, *MNRAS*, **458**, 708
- Caleb M., et al., 2017, preprint, ([arXiv:1703.10173](https://arxiv.org/abs/1703.10173))
- Carilli C. L., Ivison R. J., Frail D. A., 2003, *ApJ*, **590**, 192
- Chambers K. C., et al., 2016, preprint, ([arXiv:1612.05560](https://arxiv.org/abs/1612.05560))
- Champion D. J., et al., 2016, *MNRAS*, **460**, L30
- Chatterjee S., et al., 2017, *Nature*, **541**, 58
- Connor L., Sievers J., Pen U.-L., 2016, *MNRAS*, **458**, L19
- Cordes J. M., Lazio T. J. W., 2002, *ArXiv Astrophysics e-prints*,
- Cordes J., Wasserman I., 2016, *Monthly Notices of the Royal Astronomical Society*, **457**, 232
- Coward D. M., et al., 2017, *Publ. Astron. Soc. Australia*, **34**, e005
- Crawford D. F., Jauncey D. L., Murdoch H. S., 1970, *ApJ*, **162**, 405
- Croft S., Bower G. C., Keating G., Law C., Whysong D., Williams P. K. G., Wright M., 2011, *ApJ*, **731**, 34
- Croft S., Bower G. C., Whysong D., 2013, *ApJ*, **762**, 93
- Dhillon V. S., et al., 2014, *MNRAS*, **444**, 4009
- Diehl H. T., Dark Energy Survey Collaboration 2012, in *American Astronomical Society Meeting Abstracts #219*. p. #413.05
- Eisenstein D. J., et al., 2011, *AJ*, **142**, 72
- Evans P. A., et al., 2007, *A&A*, **469**, 379
- Evans P. A., et al., 2009, *MNRAS*, **397**, 1177
- Falcke H., Rezzolla L., 2014, *A&A*, **562**, A137
- Fialkov A., Loeb A., 2016, *J. Cosmology Astropart. Phys.*, **5**, 004
- Flaugher B. L., et al., 2012, in *Society of Photo-Optical Instrumentation Engineers (SPIE) Conference Series*. p. 11, [doi:10.1117/12.926216](https://doi.org/10.1117/12.926216)
- Flesch E. W., 2015, *Publ. Astron. Soc. Australia*, **32**, e010
- Frail D. A., et al., 1994, *ApJ*, **437**, L43
- Garrington S. T., et al., 2004, in *Oschmann Jr. J. M., ed., Proc. SPIE Vol. 5489, Ground-based Telescopes*. pp 332–343, [doi:10.1117/12.553235](https://doi.org/10.1117/12.553235)
- Gehrels N., 1986, *ApJ*, **303**, 336
- Hachenberg O., Grahl B.-H., Wielebinski R., 1973, *IEEE Proceedings*, **61**, 1288
- Hancock P. J., Murphy T., Gaensler B. M., Hopkins A., Curran J. R., 2012, *MNRAS*, **422**, 1812
- Hardy L. K., Butterley T., Dhillon V. S., Littlefair S. P., Wilson R. W., 2015, *MNRAS*, **454**, 4316
- Högbom J. A., 1974, *A&AS*, **15**, 417
- Hogg D. W., 2000, *arXiv preprint astro-ph/9905116*, 184
- Huynh M. T., Jackson C. A., Norris R. P., Prandoni I., 2005, *AJ*, **130**, 1373
- Inoue A. K., Shimizu I., Iwata I., Tanaka M., 2014, *MNRAS*, **442**, 1805
- Ioka K., 2003, *ApJL*, **598**, L79
- Ivezic Ž., et al., 2008, in *Bailer-Jones C. A. L., ed., American Institute of Physics Conference Series Vol. 1082, American Institute of Physics Conference Series*. pp 359–365 ([arXiv:0810.5155](https://arxiv.org/abs/0810.5155)), [doi:10.1063/1.3059076](https://doi.org/10.1063/1.3059076)
- Johnston S., et al., 2017, *MNRAS*, **465**, 2143
- Jurić M., et al., 2015, preprint, ([arXiv:1512.07914](https://arxiv.org/abs/1512.07914))
- Keane E. F., Petroff E., 2015, *MNRAS*, **447**, 2852
- Keane E. F., Stappers B. W., Kramer M., Lyne A. G., 2012, *MNRAS*, **425**, L71
- Keane E., et al., 2016, *Nature*, **530**, 453
- Keane E. F., et al., 2017, preprint, ([arXiv:1706.04459](https://arxiv.org/abs/1706.04459))
- Keith M. J., et al., 2010, *MNRAS*, **409**, 619
- Kulkarni S. R., Ofek E. O., Neill J. D., Zheng Z., Juric M., 2014, preprint, ([arXiv:1402.4766](https://arxiv.org/abs/1402.4766))
- Lorimer D. R., Bailes M., McLaughlin M. A., Narkevic D. J., Crawford F., 2007, *Science*, **318**, 777
- Lovell B., 1985, *The Jodrell Bank telescopes*
- Lyutikov M., Lorimer D. R., 2016, *ApJ*, **824**, L18

- Macquart J.-P., Ekers R., 2017, preprint, ([arXiv:1710.11493](https://arxiv.org/abs/1710.11493))
- Macquart J.-P., Johnston S., 2015, *MNRAS*, **451**, 3278
- Masui K., et al., 2015, preprint, ([arXiv:1512.00529](https://arxiv.org/abs/1512.00529))
- McMullin J. P., Waters B., Schiebel D., Young W., Golap K., 2007, in Shaw R. A., Hill F., Bell D. J., eds, *Astronomical Society of the Pacific Conference Series Vol. 376, Astronomical Data Analysis Software and Systems XVI*. p. 127
- Mooley K. P., Frail D. A., Ofek E. O., Miller N. A., Kulkarni S. R., Horesh A., 2013, *ApJ*, **768**, 165
- Mooley K., et al., 2016, arXiv preprint arXiv:1601.01693
- Niino Y., Totani T., Okumura J. E., 2014, *PASJ*, **66**, L9
- Ofek E., Frail D., Breslauer B., Kulkarni S., Chandra P., Gal-Yam A., Kasliwal M., Gehrels N., 2011, *The Astrophysical Journal*, **740**, 65
- Palaniswamy D., Zhang B., 2017, preprint, ([arXiv:1703.09232](https://arxiv.org/abs/1703.09232))
- Pen U.-L., Connor L., 2015, *ApJ*, **807**, 179
- Petroff E., et al., 2014, *ApJL*, **789**, L26
- Petroff E., et al., 2015a, *MNRAS*, **447**, 246
- Petroff E., et al., 2015b, *MNRAS*, **447**, 246
- Petroff E., et al., 2015c, *MNRAS*, **451**, 3933
- Petroff E., et al., 2016, preprint, ([arXiv:1601.03547](https://arxiv.org/abs/1601.03547))
- Petroff E., SUPERB Collaboration HESS Collaboration ANTARES Collaboration 2017, in *American Astronomical Society Meeting Abstracts*. p. 330.05
- Piro A. L., 2016, *ApJ*, **824**, L32
- Ransom S. M., Eikenberry S. S., Middleditch J., 2002, *AJ*, **124**, 1788
- Ravi V., Shannon R. M., Jameson A., 2015, *ApJ*, **799**, L5
- Ravi V., et al., 2016, *Science*, **354**, 1249
- Sault R. J., Teuben P. J., Wright M. C. H., 1995, in Shaw R. A., Payne H. E., Hayes J. J. E., eds, *Astronomical Society of the Pacific Conference Series Vol. 77, Astronomical Data Analysis Software and Systems IV*. p. 433 ([arXiv:astro-ph/0612759](https://arxiv.org/abs/astro-ph/0612759))
- Shannon R. M., Ravi V., 2016, preprint, ([arXiv:1611.05580](https://arxiv.org/abs/1611.05580))
- Skrutskie M. F., et al., 2006, *AJ*, **131**, 1163
- Spitler L. G., et al., 2014, *ApJ*, **790**, 101
- Spitler L., et al., 2016, *Nature*, **531**, 202
- Tendulkar S. P., et al., 2017, *ApJ*, **834**, L7
- Thornton D., et al., 2013, *Science*, **341**, 53
- Thyagarajan N., Helfand D. J., White R. L., Becker R. H., 2011, *ApJ*, **742**, 49
- Totani T., 2013, *PASJ*, **65**, L12
- Vedantham H. K., Ravi V., Hallinan G., Shannon R. M., 2016, *ApJ*, **830**, 75
- Wells D. C., 1985, in di Gesu V., Scarsi L., Crane P., Friedman J. H., Levialdi S., eds, *Data Analysis in Astronomy*. p. 195
- Wilson W. E., et al., 2011, *MNRAS*, **416**, 832
- Wright E. L., 2006, *PASP*, **118**, 1711
- Xu J., Han J. L., 2015, *Research in Astronomy and Astrophysics*, **15**, 1629
- Yao J. M., Manchester R. N., Wang N., 2017, *ApJ*, **835**, 29
- Yi S.-X., Gao H., Zhang B., 2014, *ApJ*, **792**, L21

| Telescope | UTC | T post–burst | Tobs(sec) | Sensitivity limit |
|-----------|---------------------|--------------------|--|--------------------|
| ANTARES | 2015-06-10 05:26:58 | T_{FRB} | $T_{\text{FRB}} - \text{day}; T_{\text{FRB}} + \text{day}$ | Ref. Table A10 |
| Parkes | 2017-06-08 03:22:10 | 728 days, 21:55:12 | 7200 | 466 mJy at 1.4 GHz |
| Parkes | 2017-06-08 05:26:02 | 728 days, 23:59:04 | 7200 | 466 mJy at 1.4 GHz |
| Parkes | 2017-06-08 07:38:43 | 729 days, 2:11:45 | 7200 | 466 mJy at 1.4 GHz |
| Parkes | 2017-06-08 09:43:47 | 729 days, 4:16:49 | 7200 | 466 mJy at 1.4 GHz |
| Parkes | 2017-06-08 11:48:30 | 729 days, 6:21:32 | 7200 | 466 mJy at 1.4 GHz |

Table A1. Multi-wavelength follow-up of FRB 150610 at ANTARES and Parkes. The sensitivity limits are specified for 10-sigma events with a width of 1ms at Parkes.

| Telescope | UTC | T post–burst | Tobs(sec) | Sensitivity limit |
|------------|---------------------|--------------------|--|--|
| ANTARES | 2015-12-06 06:17:52 | T_{FRB} | $T_{\text{FRB}} - \text{day}; T_{\text{FRB}} + \text{day}$ | Ref. Table A10 |
| Parkes | 2015-12-07 07:52:39 | 1 day, 1:37:43 | 120 | 466 mJy at 1.4 GHz |
| Parkes | 2015-12-07 07:55:28 | 1 day, 1:40:32 | 45.4 | 466 mJy at 1.4 GHz |
| Parkes | 2015-12-07 07:57:16 | 1 day, 1:42:20 | 830 | 466 mJy at 1.4 GHz |
| Lovell | 2015-12-07 09:49:43 | 1 day, 3:34:47 | 2982 | 350 mJy at 1.5 GHz |
| TNT | 2015-12-07 12:00:27 | 1 day, 5:45:31 | 1500 | $r' = 22.0$ |
| SRT | 2015-12-07 13:57:30 | 1 day, 7:42:34 | 12177 | 1.7 Jy at 1.5 GHz |
| e-Merlin | 2015-12-07 14:00:00 | 1 day, 7:45:04 | 18000 | 5 GHz - 204 μ Jy |
| Effelsberg | 2015-12-07 14:36:10 | 1 day, 8:21:14 | 10800 | 240 mJy at 1.4 GHz |
| SRT | 2015-12-07 15:00:00 | 1 day, 8:45:04 | 10800 | 1.7 Jy at 1.5 GHz |
| UTMOST | 2015-12-08 04:26:42 | 1 day, 22:11:46 | 13500 | 11 Jy at 843 MHz |
| Parkes | 2015-12-08 05:24:47 | 1 day, 23:09:51 | 1800 | 466 mJy at 1.4 GHz |
| Parkes | 2015-12-08 05:55:27 | 1 day, 23:40:31 | 1800 | 466 mJy at 1.4 GHz |
| Parkes | 2015-12-08 06:26:07 | 2 days, 0:11:11 | 1800 | 466 mJy at 1.4 GHz |
| Parkes | 2015-12-08 06:56:47 | 2 days, 0:41:51 | 1800 | 466 mJy at 1.4 GHz |
| Parkes | 2015-12-08 07:27:28 | 2 days, 1:12:32 | 1800 | 466 mJy at 1.4 GHz |
| Parkes | 2015-12-08 07:58:06 | 2 days, 1:43:10 | 550 | 466 mJy at 1.4 GHz |
| e-Merlin | 2015-12-08 09:30:00 | 2 days, 3:15:04 | 32400 | 204 μ Jy at 5 GHz |
| Lovell | 2015-12-08 18:09:16 | 2 days, 11:54:20 | 2985 | 350 mJy at 1.5 GHz |
| VLA | 2015-12-08 19:38:01 | 2 days, 13:23:11 | 4497 | 70 μ Jy at 5.9 GHz |
| ATCA | 2015-12-09 01:58:35 | 2 days, 19:43:39 | 10800 | 200 μ Jy at 5.5 GHz 280 μ Jy at 7.5 GHz |
| GMRT | 2015-12-09-04:15:00 | 2 days, 22:00:05 | 16200 | 180 μ Jy at 1.4 GHz |
| Lovell | 2015-12-09-17:02:04 | 3 days, 10:47:08 | 2990 | 350 mJy at 1.5 GHz |
| VLA | 2015-12-10-18:45:22 | 4 days, 12:30:26 | 4498 | 70 μ Jy at 5.9 GHz |
| TNT | 2015-12-11-11:57:22 | 5 days, 5:42:26 | 2940 | $r' = 22.0$ |
| VLA | 2015-12-12-19:22:22 | 6 days, 13:07:26 | 4498 | Badly affected by RFI |
| VLA | 2015-12-14-19:44:22 | 8 days, 13:29:26 | 4498 | 70 μ Jy 5.9 GHz |
| Lovell | 2015-12-16-17:40:27 | 10 days, 11:25:31 | 2970 | 350 mJy at 1.5 GHz |
| VLA | 2015-12-24 17:52:47 | 18 days, 11:37:51 | 4498 | 70 μ Jy at 5.9 GHz |
| VLA | 2016-01-10 16:51:57 | 35 days, 10:37:01 | 4498 | 70 μ Jy at 5.9 GHz |
| VLA | 2016-01-15 17:45:42 | 40 days, 11:30:46 | 4498 | 70 μ Jy at 5.9 GHz |
| VLA | 2016-03-06 13:39:23 | 91 days, 7:24:27 | 4328 | 70 μ Jy at 5.9 GHz |
| SRT | 2016-05-06 05:04:13 | 151 days, 22:49:17 | 10480 | 1.7 Jy at 1.5 GHz |

Table A2. Multi-wavelength follow-up of FRB 151206 at 11 telescopes. The sensitivity limits are specified for 10-sigma events with a width of 1ms at Parkes, SRT, Lovell, Effelsberg and UTMOST.

APPENDICES

A FRB follow-up summary

Tables A1 to A4 below summarise all of the follow-up observations that have been performed for the four FRBs presented in this paper.

| Telescope | UTC | T post-burst | Tobs(sec) | Sensitivity limit |
|-----------|---------------------|-------------------|--|---|
| ANTARES | 2015-12-30 17:03:26 | T_{FRB} | $T_{\text{FRB}} - \text{day}; T_{\text{FRB}} + \text{day}$ | Ref. Table A10 |
| Zadko | 2015-12-30 18:03:21 | 00:59:55 | 7457 | $r < 19.8$ |
| Parkes | 2015-12-30 18:03:30 | 01:00:04 | 3616.01 | 466 mJy at 1.4 GHz |
| Parkes | 2015-12-30 19:32:28 | 02:29:02 | 3618.11 | 466 mJy at 1.4 GHz |
| SWIFT | 2015-12-30 23:14:45 | 06:11:19 | 2056.5 | $1.918 \times 10^{13} \text{ erg}^{-1} \text{ cm}^2 \text{ s}^{-1}$ |
| DECam | 2015-12-31 07:11:17 | 14:07:51 | 900 | $u < 21.5$ |
| DECam | 2015-12-31 07:28:42 | 14:25:16 | 375 | $g < 22.5$ |
| DECam | 2015-12-31 07:37:22 | 14:33:56 | 200 | $r < 23.8$ |
| DECam | 2015-12-31 07:43:06 | 14:39:40 | 750 | $i < 24.1$ |
| ATCA | 2015-12-31 14:15:45 | 21:12:19 | 28800 | 288 μJy at 5.5 GHz 348 μJy at 7.5 GHz |
| Lovell | 2016-01-01 00:44:43 | 1 day, 7:41:17 | 7200 | 350 mJy at 1.5 GHz |
| DECam | 2016-01-01 07:44:44 | 1 day, 14:41:18 | 200 | $g < 22.6$ |
| Parkes | 2016-01-01 13:42:56 | 1 day, 20:39:30 | 3619.95 | 466 mJy at 1.4 GHz |
| Parkes | 2016-01-01 14:43:39 | 1 day, 21:40:13 | 3617.06 | 466 mJy at 1.4 GHz |
| Parkes | 2016-01-01 15:44:19 | 1 day, 22:40:53 | 3617.06 | 466 mJy at 1.4 GHz |
| Parkes | 2016-01-01 16:45:09 | 1 day, 23:41:43 | 3617.06 | 466 mJy at 1.4 GHz |
| Parkes | 2016-01-01 17:45:49 | 2 days, 0:42:23 | 3617.06 | 466 mJy at 1.4 GHz |
| Parkes | 2016-01-01 18:46:28 | 2 days, 1:43:02 | 3618.11 | 466 mJy at 1.4 GHz |
| Parkes | 2016-01-01 19:47:09 | 2 days, 2:43:43 | 3617.06 | 466 mJy at 1.4 GHz |
| Parkes | 2016-01-02 14:20:00 | 2 days, 21:16:34 | 3616.01 | 466 mJy at 1.4 GHz |
| Parkes | 2016-01-02 15:20:38 | 2 days, 22:17:12 | 3618.11 | 466 mJy at 1.4 GHz |
| Parkes | 2016-01-02 16:21:18 | 2 days, 23:17:52 | 3618.11 | 466 mJy at 1.4 GHz |
| Parkes | 2016-01-02 17:22:10 | 3 days, 0:18:44 | 3616.01 | 466 mJy at 1.4 GHz |
| Parkes | 2016-01-02 18:22:47 | 3 days, 1:19:21 | 3618.9 | 466 mJy at 1.4 GHz |
| Parkes | 2016-01-02 19:23:28 | 3 days, 2:20:02 | 3618.11 | 466 mJy at 1.4 GHz |
| Parkes | 2016-01-03 13:32:51 | 3 days, 20:29:25 | 3624.93 | 466 mJy at 1.4 GHz |
| Parkes | 2016-01-03 14:33:38 | 3 days, 21:30:12 | 3618.11 | 466 mJy at 1.4 GHz |
| Parkes | 2016-01-03 15:34:19 | 3 days, 22:30:53 | 3617.06 | 466 mJy at 1.4 GHz |
| Parkes | 2016-01-03 16:35:09 | 3 days, 23:31:43 | 3617.06 | 466 mJy at 1.4 GHz |
| Parkes | 2016-01-03 17:35:48 | 4 days, 0:32:22 | 3618.11 | 466 mJy at 1.4 GHz |
| Lovell | 2016-01-03 22:41:31 | 4 days, 5:38:05 | 5580 | 350 mJy at 1.5 GHz |
| Lovell | 2016-01-04 00:16:07 | 4 days, 7:12:41 | 1596 | 350 mJy at 1.5 GHz |
| Parkes | 2016-01-04 14:54:30 | 4 days, 21:51:04 | 3616.01 | 466 mJy at 1.4 GHz |
| Parkes | 2016-01-04 15:55:10 | 4 days, 22:51:44 | 3616.01 | 466 mJy at 1.4 GHz |
| Parkes | 2016-01-04 16:56:00 | 4 days, 23:52:34 | 3616.01 | 466 mJy at 1.4 GHz |
| Parkes | 2016-01-04 17:58:08 | 5 days, 0:54:42 | 3618.11 | 466 mJy at 1.4 GHz |
| Parkes | 2016-01-04 18:58:49 | 5 days, 1:55:23 | 1258.03 | 466 mJy at 1.4 GHz |
| Parkes | 2016-01-04 19:20:18 | 5 days, 2:16:52 | 3618.11 | 466 mJy at 1.4 GHz |
| Parkes | 2016-01-05 14:40:00 | 5 days, 21:36:34 | 3616.01 | 466 mJy at 1.4 GHz |
| Parkes | 2016-01-05 15:40:39 | 5 days, 22:37:13 | 3617.06 | 466 mJy at 1.4 GHz |
| Parkes | 2016-01-05 16:41:42 | 5 days, 23:38:16 | 3623.88 | 466 mJy at 1.4 GHz |
| Parkes | 2016-01-05 17:43:03 | 6 days, 0:39:37 | 3623.09 | 466 mJy at 1.4 GHz |
| Parkes | 2016-01-05 18:52:06 | 6 days, 1:48:40 | 3619.95 | 466 mJy at 1.4 GHz |
| Parkes | 2016-01-06 14:41:36 | 6 days, 21:38:10 | 3619.95 | 466 mJy at 1.4 GHz |
| Parkes | 2016-01-06 15:42:16 | 6 days, 22:38:50 | 3619.95 | 466 mJy at 1.4 GHz |
| Parkes | 2016-01-06 16:43:10 | 6 days, 23:39:44 | 3616.01 | 466 mJy at 1.4 GHz |
| Parkes | 2016-01-06 17:43:47 | 7 days, 0:40:21 | 3618.9 | 466 mJy at 1.4 GHz |
| Parkes | 2016-01-06 18:48:33 | 7 days, 1:45:07 | 3623.09 | 466 mJy at 1.4 GHz |
| GMRT | 2016-01-06 18:30:00 | 7 days, 1:26:34 | 15588 | 180 μJy at 1.4 GHz |
| Parkes | 2016-01-06 19:53:13 | 7 days, 2:49:47 | 1900.28 | 466 mJy at 1.4 GHz |
| Subaru | 2016-01-07 11:23:19 | 7 days, 18:19:53 | 4200 | Refer table A7 |
| Subaru | 2016-01-07 13:17:22 | 7 days, 20:13:56 | 3150 | Refer table A7 |
| Subaru | 2016-01-07 15:12:39 | 7 days, 22:09:13 | 4200 | Refer table A7 |
| Subaru | 2016-01-10 11:11:39 | 10 days, 18:08:13 | 3600 | Refer table A7 |
| Subaru | 2016-01-10 13:03:29 | 10 days, 20:00:03 | 3600 | Refer table A7 |
| Subaru | 2016-01-10 15:07:20 | 10 days, 22:03:54 | 4080 | Refer table A7 |
| ATCA | 2016-01-11 11:36:55 | 11 days, 18:33:29 | 34440 | 288 μJy at 5.5 GHz 390 μJy at 7.5 GHz |

| Telescope | UTC | T post–burst | Tobs(sec) | Sensitivity limit |
|-----------|---------------------|-------------------|-----------|--|
| Subaru | 2016-01-13 11:21:54 | 13 days, 18:18:28 | 3600 | Refer table A7 |
| UTMOST | 2016-01-13 12:13:48 | 13 days, 19:10:22 | 27000 | 11 Jy at 843 MHz |
| Subaru | 2016-01-13 13:12:52 | 13 days, 20:09:26 | 3600 | Refer table A7 |
| Subaru | 2016-01-13 15:13:35 | 13 days, 22:10:09 | 3600 | Refer table A7 |
| Lovell | 2016-01-14 00:03:12 | 14 days, 6:59:46 | 7200 | 350 mJy at 1.5 GHz |
| Lovell | 2016-01-30 00:32:04 | 30 days, 7:28:38 | 7200 | 350 mJy at 1.5 GHz |
| GMRT | 2016-02-17 19:30:00 | 49 days, 2:26:34 | 14400 | 180 μJy at 1.4 GHz |
| ATCA | 2016-02-24 09:48:15 | 55 days, 16:44:49 | 16500 | 240 μJy at 5.5 GHz 252 μJy at 7.5 GHz |
| VLA | 2016-02-29 06:42:11 | 60 days, 13:38:45 | 4353 | 105 μJy at 5.9 GHz |
| GMRT | 2016-03-03 13:30:00 | 63 days, 20:26:34 | 14400 | 180 μJy at 1.4 GHz |
| VLA | 2016-03-04 06:26:25 | 64 days, 13:22:59 | 4353 | 84 μJy at 5.9 GHz |
| Lovell | 2016-03-18 18:34:51 | 79 days, 1:31:25 | 1965 | 350 mJy at 1.5 GHz |
| SRT | 2016-05-10 17:58:43 | 132 days, 0:55:17 | 10350 | 1.7 Jy at 1.5 GHz |

Table A3. Multi-wavelength follow-up of FRB 151230 at 12 telescopes. The sensitivity limits are specified for 10-sigma events with a width of 1ms at Parkes, SRT, Lovell and UTMOST.

| Telescope | UTC | T post–burst | Tobs (sec) | Sensitivity limit |
|-----------|---------------------|--------------------|--|---|
| ANTARES | 2016-01-02 08:28:38 | T_{FRB} | $T_{\text{FRB}} - \text{day}; T_{\text{FRB}} + \text{day}$ | Ref. Table A10 |
| Parkes | 2016-01-02 09:44:28 | 01:15:50 | 3618.11 | 466 mJy at 1.4 GHz |
| SWIFT | 2016-01-02 13:05:17 | 04:36:39 | 3582 | $1.434 \times 10^{13} \text{ erg}^{-1} \text{ cm}^2 \text{ s}^{-1}$ |
| ATCA | 2016-01-03 02:42:45 | 18:14:07 | 14400 | 420 μJy at 5.5 GHz 450 μJy at 7.5 GHz |
| Parkes | 2016-01-03 03:23:01 | 18:54:23 | 3624.93 | 466 mJy at 1.4 GHz |
| Parkes | 2016-01-03 04:23:47 | 19:55:09 | 3618.9 | 466 mJy at 1.4 GHz |
| Parkes | 2016-01-03 05:50:16 | 21:21:38 | 3619.95 | 466 mJy at 1.4 GHz |
| Parkes | 2016-01-03 06:51:11 | 22:22:33 | 3624.93 | 466 mJy at 1.4 GHz |
| Parkes | 2016-01-03 08:15:34 | 23:46:56 | 3622.04 | 466 mJy at 1.4 GHz |
| Parkes | 2016-01-03 09:16:18 | 1 day, 0:47:39 | 3618.11 | 466 mJy at 1.4 GHz |
| Parkes | 2016-01-03 10:16:59 | 1 day, 1:48:21 | 1556.87 | 466 mJy at 1.4 GHz |
| Parkes | 2016-01-04 10:18:14 | 2 days, 1:49:35 | 1179.39 | 466 mJy at 1.4 GHz |
| SWIFT | 2016-01-05 06:04:58 | 2 days, 21:36:20 | 1827 | $1.966 \times 10^{13} \text{ erg}^{-1} \text{ cm}^2 \text{ s}^{-1}$ |
| Parkes | 2016-01-06 09:11:36 | 4 days, 0:42:57 | 3619.95 | 466 mJy at 1.4 GHz |
| Parkes | 2016-01-06 10:12:17 | 4 days, 1:43:38 | 896.27 | 466 mJy at 1.4 GHz |
| ATCA | 2016-01-11 05:34:35 | 8 days, 21:05:57 | 21060 | 330 μJy at 5.5 GHz 360 μJy at 7.5 GHz |
| UTMOST | 2016-01-13 06:43:00 | 10 days, 22:14:22 | 16920 | 11 Jy at 843 MHz |
| SWIFT | 2016-02-04 22:12:06 | 33 days, 13:43:28 | 3349 | $1.491 \times 10^{13} \text{ erg}^{-1} \text{ cm}^2 \text{ s}^{-1}$ |
| GMRT | 2016-02-06 06:30:00 | 34 days, 22:01:22 | 14400 | 180 μJy at 1.4 GHz |
| ATCA | 2016-02-24 02:40:05 | 52 days, 18:11:27 | 23400 | 240 μJy at 5.5 GHz 300 μJy at 7.5 GHz |
| VLA | 2016-02-26 17:50:17 | 55 days, 9:21:39 | 4283 | 70 μJy at 5.9 GHz |
| VLA | 2016-03-04 17:14:41 | 62 days, 8:46:03 | 4283 | 70 μJy at 5.9 GHz |
| SRT | 2016-05-07 07:52:08 | 125 days, 23:23:30 | 7200 | 1.7 Jy at 1.5 GHz |

Table A4. Multi-wavelength follow-up of FRB 160102 at 8 telescopes. The sensitivity limits are specified for 10-sigma events with a width of 1ms at Parkes, SRT and UTMOST.

B Interferometric observational details and variability criteria

Table A5 summarises the observations performed by the ATCA, VLA and GMRT on the field of SUPERB FRBs. For all detected sources the following statistics were used to test for variability using a method very similar to Bell et al. (2015). Firstly, the chi-square χ^2 probability that the source is not variable is estimated with:

$$\chi^2 = \sum_{i=1}^n \frac{(S_i - \bar{S}_{\text{wt}})^2}{\sigma_i^2} \quad (6)$$

where S_i is the flux value in an epoch i , σ_i is the inverse of individual error in the flux measurement and \bar{S}_{wt} is the weighted mean flux. Using χ^2 distribution tables for $n - 1$ degrees of freedom, a source is classified as variable if $P < 0.001$ where P is the probability that χ^2 is

Table A5. Radio imaging observations performed with the ATCA, VLA and GMRT on the field of SUPERB FRBs. The table lists the number of epochs, area covered and primary & secondary calibrators used for these observations.

| | ATCA | | | | VLA | | | | GMRT | | | |
|------------|---------------|--------------------------|----------|----------|---------------|--------------------------|---------|------------|---------------|--------------------------|---------|----------|
| | No. of epochs | Area (deg ²) | PC & SC | | No. of epochs | Area (deg ²) | PC & SC | | No. of epochs | Area (deg ²) | PC & SC | |
| FRB 151260 | 1 | 0.05 | 1934–638 | 1937–101 | 8 | 0.05 | 3C286 | J2355+4950 | 1 | 0.05 | 3C286 | 2011–067 |
| FRB 151230 | 3 | 0.05 | 1934–638 | 0941–080 | 2 | 0.05 | 3C138 | J0943–0819 | 3 | 0.05 | 3C48 | 0943–083 |
| FRB 160102 | 3 | 0.2 | 1934–638 | 2240–260 | 2 | 0.05 | 3C48 | J2248–3235 | 1 | 0.2 | 3C48 | 3C286 |

produced by chance. Additionally, the de-biased modulation index is calculated using:

$$m_d = \frac{1}{\bar{S}} \sqrt{\frac{\sum_{i=1}^n (S_i - \bar{S})^2 - \sum_{i=1}^n \sigma_i^2}{n}} \quad (7)$$

where \bar{S} is the mean flux density. Lastly, the fractional variability is computed using:

$$\Delta S = \frac{S_{\max} - S_{\min}}{\bar{S}}, \quad (8)$$

where S_{\max} and S_{\min} are the maximum and minimum flux densities for a source over n epochs. A source is regarded to be a significant variable if the χ^2 is greater than threshold χ_{thresh}^2 and $\Delta S > 50\%$, similar to Bell et al. (2015).

B.1 The Australian Telescope Compact Array

The follow-up of three of the FRB fields was performed with the ATCA, using compact array broadband backend (CABB) (Wilson et al. 2011) with a bandwidth of 2 GHz each centred at 5.5 GHz and 7.5 GHz to search for radio afterglows or variable sources associated with FRBs. The observations were done in a 42 pointing mosaic mode encompassing the localisation error radius of 7.5'. The data were reduced following the standard steps of imaging in *miriad* (Sault et al. 1995). *Aegean* (Hancock et al. 2012) was used as a source finding and flux estimation software along with *miriad* tasks *IMRAD* and *IMFIT*. The images were searched for sources down to the threshold of 6-sigma in all ATCA data and a variability analysis (described above) was performed to identify variable sources.

B.2 The Karl G. Jansky VLA

The VLA observations were performed in the 4 GHz to 8 GHz band with a centre frequency of 5.9 GHz. A seven pointing mosaic was done to encompass Parkes localisation error radius of 7.5'. The data reduction was performed using CASA (McMullin et al. 2007). All sources detected above 7-sigma were monitored between the epochs to search for variable sources. We note here that the flux density scale using wide-band VLA mosaics is unreliable due to poorly constrained primary beam shape over the wide frequency band, however the flux scale is stable between epochs such that although the absolute flux scale of the mosaic images is wrong, the variability analysis will be correct.

B.3 The Giant Metrewave Radio Telescope

The GMRT (Ananthakrishnan 1995) observed the FRB fields at the center frequency of 1.4 GHz and bandwidth of 120 MHz. The data reduction was performed using the data reduction software AIPS (Wells 1985). *Aegean* was used as source finding algorithm and a search for sources was performed down to 6-sigma noise level.

B.4 e-Merlin radio telescope

The follow-up of FRB 151206 was also conducted by the e-Merlin telescope (Garrington et al. 2004) with a bandwidth of 512 MHz centred on 5072.3 MHz. The data reduction was done using software AIPS (Wells 1985) and a search for sources was performed down to 6-sigma noise limit.

C Observational details and magnitude limits for non radio follow-ups.

C.1 Thai National Telescope

Optical follow up imaging was conducted on the field of FRB 151206 with the 2.4m Thai National Telescope (TNT), using the ULTRASPEC camera, with field of view 8' × 8' (Dhillon et al. 2014). Four tilings were observed on the night of 2015 December 7. Each tile observation consisted of 6 r'-band images with exposure times of 60 seconds. The same 4 tiles were repeated 4 days later, enabling a comparative analysis of sources. The effective overlapping area observed on both occasions was 15' × 15', centred on 19:21:27, -04:07:35 (J2000). The estimated 5-sigma detection limits for both epochs were $r' = 22.0$. The variable sources detected are presented in Table A6.

Table A6. Optical variable sources detected by the Thai National Telescope (TNT) in the field of FRB 151206.

| RA | DEC | r' mag | Δ mag |
|-------------|-------------|----------|--------------|
| 19:21:28.47 | -04:08:50.5 | 17.8 | +0.5 |
| 19:21:50.00 | -04:13:38.2 | 17.9 | +0.2 |
| 19:21:01.30 | -04:12:00.4 | 18.3 | +0.2 |
| 19:21:07.99 | -04:11:38.7 | 15.2 | -0.1 |

Table A7. Limiting magnitudes for Subaru observations of FRB 151230 field.

| Band | 2016-01-07 - 2016-01-13 | 2016-01-10 - 2016-01-13 |
|-------|-------------------------|-------------------------|
| HSC-G | >26.1 | >26.3 |
| HSC-R | >25.8 | >25.8 |
| HSC-I | >26.00 | >26.1 |

Table A8. Details of the follow up of FRB 151230 performed with DECam, including the date and time of the observation, the filter used, the individual exposure time, and the number of exposures N_{exp} taken with a regular dithering pattern.

| Obs. time (UTC) | Filter | Exp (s) | N_{exp} |
|------------------------|----------|---------|------------------|
| 2015-12-31, 07:11:17.1 | <i>i</i> | 180 | 5 |
| 2015-12-31, 07:28:42.5 | <i>r</i> | 75 | 5 |
| 2015-12-31, 07:37:22.2 | <i>g</i> | 40 | 5 |
| 2015-12-31, 07:43:06.8 | <i>u</i> | 150 | 5 |
| 2016-01-01, 07:44:44.4 | <i>g</i> | 40 | 5 |

C.2 Subaru Telescope

The Hyper Suprime-Cam (HSC) data are reduced using HSC pipeline version 4.0.5 (Bosch et al. 2017), which is developed based on the LSST pipeline (Ivezic et al. 2008; Axelrod et al. 2010; Jurić et al. 2015), in the usual manner including bias subtraction, flat-fielding, astrometry, flux calibration, mosaicing, warping, coadding, and image subtraction. The astrometric and photometric calibration is made relative to the Pan-STARRS1 (Chambers et al. 2016) with a 4.0 (24 pixel) aperture diameter.

For transient finding, the HSC pipeline adopts the frequently used image subtraction algorithm developed by Alard (2000) and Alard & Lupton (1998); an image with narrower point spread functions (PSFs) are convolved with spatially varying kernels to match the wider PSFs of the other image, and the image subtraction is made for the PSF-matched images. In the analysis, we set the images taken on Jan 13 as the reference images and are subtracted from the science images taken on Jan 7 and 10. The 5-sigma limiting magnitude on the variability are estimated by 1000 – 4000 apertures with a diameter being twice as large as the FWHM size of PSF. The apertures are randomly sampled from positions without any detection in the science and reference images and are locally sky subtracted.

Since the detected sources include many fakes, transient candidates are further selected using their measured properties and the spatially varying PSF and elongation of the difference images. We select the transient candidates detected at least twice with the following detection criteria; (1) the detection significance is higher than 5-sigma, (2) the PSF size is between 0.8 and 1.3 of PSF size of the difference image, (3) the elongation is larger than 0.65 of elongation of the difference image, and (4) the residual of the subtraction of the PSF kernel from the detected source is less than 3-sigma. The limiting magnitudes for Subaru observations are listed in Table A7.

C.3 DECam

The Dark Energy Camera (DECam; Diehl & Dark Energy Survey Collaboration 2012; Flaugher et al. 2012) is a wide-field optical imager mounted at the primary focus of the 4-m Blanco telescope at CTIO. Table A8 and A9 summarises the details of these observations and the limiting magnitudes

The radio sources in ATCA and GMRT images for the FRB 151230 field were compared with DECam optical image to look for optical counterparts. Optical sources present above 5-sigma of the background noise are considered to be a detection in each *u-g-r-i* filter. We found that 52% of the radio sources have an optical counterpart in at least one filter, for a search radius of 3 arcsec. This result of radio-to-optical source association is consistent with the work of Huynh et al. (2005).

C.4 The Zadko Telescope

The Zadko Telescope (Coward et al. 2017) is a 1 m f/4 Cassegrain telescope situated in the state of Western Australia. The Zadko telescope has a moderate field of view of $23' \times 23'$, so the complete shadowing of the Parkes multi-beam receiver required 5-tile images.

Table A9. Detection limits (AB magnitudes) for sources detected in the DECam images for the field of FRB 151230 with significance reported in the last column. Refer to Table A8 for more details about the observations.

| Detection limits | | | |
|------------------|----------------------|------------|-----------|
| filter | Date | < mag (AB) | $N\sigma$ |
| <i>u</i> | Dec 31 st | 21.52 | 5 |
| <i>g</i> | Dec 31 st | 23.37 | 5 |
| | | 22.55 | 10 |
| <i>g</i> | Jan 1 st | 23.53 | 5 |
| | | 22.68 | 10 |
| <i>r</i> | Dec 31 st | 23.84 | 5 |
| <i>i</i> | Dec 31 st | 24.17 | 5 |

Table A10. Upper limits on the neutrino fluence, $F_{\nu,90\%}$, estimated for the 4 FRBs according to the instantaneous ANTARES sensitivity. The limits are given in the energy range $[E_{\min} - E_{\max}]$ where 90% of the neutrino signal is expected.

| FRB | $\frac{dN}{dE_{\nu}} \propto E_{\nu}^{-2}$ | | $\frac{dN}{dE_{\nu}} \propto E_{\nu}^{-1}$ | |
|--------|--|---|--|---|
| | $F_{\nu,90\%}$ erg · cm ⁻² (GeV · cm ⁻²) | $[E_{\min}; E_{\max}]$ log ₁₀ [GeV] | $F_{\nu,90\%}$ erg · cm ⁻² (GeV · cm ⁻²) | $[E_{\min}; E_{\max}]$ log ₁₀ [GeV] |
| 150610 | $3.2 \cdot 10^{-2}$ (20) | [3.4; 6.8] | 2.54 (1600) | [5.8; 7.9] |
| 151206 | $1.8 \cdot 10^{-2}$ (11) | [3.6; 6.9] | 0.41 (250) | [5.8; 8.0] |
| 151230 | $1.8 \cdot 10^{-2}$ (11) | [3.2; 6.8] | 0.76 (470) | [5.8; 8.0] |
| 160102 | $2.6 \cdot 10^{-2}$ (16) | [3.6; 7.0] | 0.47 (290) | [5.8; 8.0] |

C.5 The ANTARES neutrino detector

Searches for up-going track events in the ANTARES data have been optimised to give a 3-sigma discovery potential for one neutrino event in a search time window of $\Delta T = [T_0 - 6 \text{ hr}; T_0 + 6 \text{ hr}]$ within the ROI. For the four FRBs, the expected background event rate in a ROI of 2° is of the order of $R_{\mu} \sim 5 \cdot 10^{-8} \text{ event} \cdot \text{s}^{-1}$. Thus, the Poisson probability of observing zero event, knowing the background event rate, is $\geq 99\%$ for any of the four FRBs. Hence, the null result is compatible with the background expectation.

The non detection of neutrino counterparts allows to derive upper limits at 90% confidence level on the neutrino fluence of the four FRBs based on the instantaneous acceptance of ANTARES at the FRB trigger time: $F_{\nu,90\%} < \int_{E_{\min}}^{E_{\max}} dN/dE_{\nu} \cdot E_{\nu} \cdot dE_{\nu}$. Two generic neutrino energy spectra were considered and defined by a power law function $dN/dE_{\nu} \propto E_{\nu}^{-\Gamma}$ with spectral indices $\Gamma = 1$ and 2. The limits are then computed using a dedicated Monte Carlo simulation that takes into account the response of the detector at the FRB trigger time. The energy range $[E_{\min}; E_{\max}]$ corresponds to the 5-95% range of the energy distribution of the events in the optimised dataset. The results on the neutrino fluence upper limits for the two considered neutrino spectra are given in Table A10. Constraints on the isotropic energy released in neutrinos can be set depending on the distance of the considered FRB: $E_{\nu,90\%}^{\text{iso}} = 4\pi D^2 \cdot F_{\nu,90\%}/(1+z)$, where D is the effective distance travelled by the neutrinos. For the E_{ν}^{-2} spectral model, three FRB distance scenarios have been tested: a galactic environment with $D = 50 \text{ kpc}$ ($z \sim 0$), a nearby extragalactic distance with $D = 100 \text{ Mpc}$ ($z \sim 0.02$) and a cosmological scenario with $D = D(z)$ depending on the cosmological parameters and the maximum z inferred from DM as listed in Table 1. The cosmological distance, $D(z)$, travelled by the neutrinos from each FRB was computed from the Eq. 4 of Adrian-Martínez et al. (2016) and found to be $D(z) = 6.61, 6.75, 3.67, 10.17 \text{ Gpc}$ respectively. For the four FRBs, the ANTARES constraints given by $E_{\nu,90\%}^{\text{iso}}$ are at the level of $E_{\nu,90\%}^{\text{iso}} \sim 10^{45}, 10^{52}$ and 10^{55} erg , respectively for the three distance scenarios. In particular, if these four FRBs are associated with neutrino emission following a E_{ν}^{-2} spectrum and with $E_{\nu,90\%}^{\text{iso}} \gtrsim 10^{52} \text{ erg}$, ANTARES excludes their origin at distance within 100 Mpc.

THE ANTARES COLLABORATION

A. Albert³², M. André³³, M. Anghinolfi³⁴, G. Anton³⁵, M. Ardid³⁶, J.-J. Aubert³⁷, T. Avgitis³⁸, B. Baret³⁸, J. Barrios-Martí³⁹, S. Basa⁴⁰, B. Belhorma⁴¹, V. Bertin³⁷, S. Biagi⁴², R. Bormuth^{43,44}, S. Bourret³⁸, M.C. Bouwhuis⁴³, H. Brânzaş⁴⁵, R. Bruijn^{43,46}, J. Brunner³⁷, J. Busto³⁷, A. Capone^{47,48}, L. Caramete⁴⁵, J. Carr³⁷, S. Celli^{47,48,49}, R. Cherkaoui El Moursli⁵⁰, T. Chiarusi⁵¹, M. Circella⁵², J.A.B. Coelho³⁸, A. Coleiro^{38,39}, R. Coniglione⁴², H. Costantini³⁷, P. Coyle³⁷, A. Creusot³⁸, A. F. Díaz⁵³, A. Deschamps⁵⁴, G. De Bonis^{47,48}, C. D'Este⁴², I. Di Palma^{47,48}, A. Domi^{34,55}, C. Donzaud^{38,56}, D. Dornic³⁷, D. Drouhin³², T. Eberl³⁵, I. El Bojaddaini⁵⁷, N. El Khayati⁵⁰, D. Elsässer⁵⁸, A. Enzenhöfer³⁷, A. Ettahiri⁵⁰, F. Fassi⁵⁰, I. Felis³⁶, L.A. Fusco^{51,59}, P. Gay^{60,38}, V. Giordano⁶¹, H. Glotin^{62,63}, T. Gregoire³⁸, R. Gracia-Ruiz³⁸, K. Graf³⁵, S. Hallmann³⁵, H. van Haren⁶⁴, A.J. Heijboer⁴³, Y. Hello⁵⁴, J.J. Hernández-Rey³⁹, J. Höflich³⁵, J. Hofstadter³⁵, C. Hugon^{34,59}, G. Illuminati³⁹, C.W. James³⁵, M. de Jong^{43,44}, M. Jongen⁴³, M. Kadler⁵⁸, O. Kalekin³⁵, U. Katz³⁵, D. Kießling³⁵, A. Kouchner^{38,63}, M. Kreter⁵⁸, I. Kreykenbohm⁶⁵, V. Kulikovskiy^{37,66}, C. Lachaud³⁸, R. Lahmann³⁵, D. Lefèvre⁶⁷, E. Leonora^{61,68}, S. Loucatos^{69,38}, M. Marcellin⁴⁰, A. Margiotta^{51,59}, A. Marinelli^{70,71}, J.A. Martínez-Mora³⁶, R. Mele^{72,73}, K. Melis^{43,46}, T. Michael⁴³, P. Migliozi⁷², A. Mousa⁵⁷, S. Navas⁷⁴, E. Nezri⁴⁰, M. Organokov⁷⁵, G.E. Pávlas⁴⁵, C. Pellegrino^{51,59}, C. Perrina^{47,48}, P. Piattelli⁴², V. Popa⁴⁵, T. Pradier⁷⁵, L. Quinn³⁷, C. Racca³², G. Riccobene⁴², A. Sánchez-Losa⁵², M. Saldaña³⁶, I. Salvadori³⁷, D. F. E. Samtleben^{43,44}, M. Sanguineti^{34,55}, P. Sapienza⁴², F. Schüssler⁶⁹, C. Sieger³⁵, M. Spurio^{51,59}, Th. Stolarczyk⁶⁹, M. Taitui^{34,55}, Y. Tayalati⁵⁰, A. Trovato⁴², D. Turpin³⁷, C. Tönnis³⁹, B. Vallage^{69,38}, V. Van Elewyck^{38,63}, F. Versari^{51,59}, D. Vivolo^{72,73}, A. Vizzocca^{47,48}, J. Wilms⁶⁵, J.D. Zornoza³⁹, J. Zúñiga³⁹

¹Centre for Astrophysics and Supercomputing, Swinburne University of Technology, Mail H30, PO Box 218, VIC 3122, Australia

²ARC Centre of Excellence for All-sky Astrophysics (CAASTRO)

³CSIRO Astronomy & Space Science, Australia Telescope National Facility, P.O. Box 76, Epping, NSW 1710, Australia

⁴SKA Organisation, Jodrell Bank Observatory, Cheshire, SK11 9DL, UK

⁵ASTRON, The Netherlands Institute for Radio Astronomy, Postbus 2, 7990 AA Dwingeloo, The Netherlands

⁶National Radio Astronomy Observatory, 1003 Lopezville Rd., Socorro, NM 87801, USA

⁷Department of Physics and Astronomy, West Virginia University, P.O. Box 6315, Morgantown, WV 26506, USA; Center for Gravitational Waves and Cosmology, West Virginia University, Chestnut Ridge Research Building, Morgantown, WV 26505

⁸Australian Astronomical Observatory, 105 Delhi Rd, North Ryde, NSW 2113, Australia.

⁹Max Planck Institut für Radioastronomie, Auf dem Hügel 69, D-53121 Bonn, Germany

¹⁰International Centre for Radio Astronomy Research, Curtin University, Bentley, WA 6102, Australia

¹¹INAF-Osservatorio Astronomico di Cagliari, Via della Scienza 5, I-09047 Selargius (CA), Italy.

¹²Research School of Astronomy and Astrophysics, Australian National University, ACT, 2611, Australia

¹³National Centre for Radio Astrophysics, Tata Institute of Fundamental Research, Pune University Campus, Ganeshkhind, Pune 411 007, India

¹⁴Department of Physics and Astronomy, University of Sheffield, Sheffield S3 7RH, UK

¹⁵Jodrell Bank Centre for Astrophysics, University of Manchester, Alan Turing Building, Oxford Road, Manchester M13 9PL, United Kingdom

¹⁶Fakultät für Physik, Universität Bielefeld, Postfach 100131, D-33501 Bielefeld, Germany

¹⁷Institute for Radio Astronomy and Space Research, Auckland University of Technology, 120 Mayoral Drive, Auckland 1010, New Zealand

¹⁸University of British Columbia, 2329 West Mall, Vancouver, BC V6T 1Z4, Canada

¹⁹Konan University, 8-9-1 Okamoto, Higashinada Ward, Kobe, Hyogo Prefecture 658-0072, Japan

²⁰University of Tokyo, 7 Chome-3-1 Hongo, Bunkyo, Tokyo 113-8654, Japan

²¹School of Physics, University of Western Australia, M013, Crawley WA 6009, Australia

²²Université de Toulouse; UPS-OMP; IRAP; Toulouse, France

²³CNRS; IRAP; 14, avenue Edouard Belin, F-31400 Toulouse, France

²⁴International Centre for Radio Astronomy Research, M468, The University of Western Australia, Crawley, WA 6009, Australia

²⁵Subaru Telescope, National Astronomical Observatory of Japan, 650 North A'ohoku Place, Hilo, HI 96720, USA

²⁶National Astronomical Observatory of Japan, 2-21-1 Osawa, Mitaka, Tokyo 181-8588, Japan

²⁷Instituto de Astrofísica de Canarias, E-38205 La Laguna, Tenerife, Spain

²⁸Department of Physics, University of Warwick, Coventry CV4 7AL, UK

²⁹Center for Advanced Instrumentation, Department of Physics, University of Durham, South Road, Durham DH1 3LE, UK

³⁰National Astronomical Research Institute of Thailand, 191 Siriraphich Building, Huay Kaew Road, Chiang Mai 50200, Thailand

³¹Kavli Institute for the Physics and Mathematics of the Universe (WPI), The University of Tokyo, 5-1-5 Kashiwanoha, Kashiwa, Chiba 277-8583, Japan

³²GRPHE - Université de Haute Alsace - Institut universitaire de technologie de Colmar, 34 rue du Grillenbreit BP 50568 - 68008 Colmar, France

³³Technical University of Catalonia, Laboratory of Applied Bioacoustics, Rambla Exposició, 08800 Vilanova i la Geltrú, Barcelona, Spain

³⁴INFN - Sezione di Genova, Via Dodecaneso 33, 16146 Genova, Italy

³⁵Friedrich-Alexander-Universität Erlangen-Nürnberg, Erlangen Centre for Astroparticle Physics, Erwin-Rommel-Str. 1, 91058 Erlangen, Germany

³⁶Institut d'Investigació per a la Gestió Integrada de les Zones Costaneres (IGIC) - Universitat Politècnica de València. C/ Paranimf 1, 46730 Gandia, Spain

³⁷Aix Marseille Univ, CNRS/IN2P3, CPPM, Marseille, France

³⁸APC, Univ Paris Diderot, CNRS/IN2P3, CEA/Irfu, Obs de Paris, Sorbonne Paris Cité, France

³⁹IFIC - Instituto de Física Corpuscular (CSIC - Universitat de València) c/ Catedrático José Beltrán, 2 E-46980 Paterna, Valencia, Spain

⁴⁰LAM - Laboratoire d'Astrophysique de Marseille, Pôle de l'Étoile Site de Château-Gombert, rue Frédéric Joliot-Curie 38, 13388 Marseille Cedex 13, France

⁴¹National Center for Energy Sciences and Nuclear Techniques, B.P.1382, R. P.10001 Rabat, Morocco

⁴²INFN - Laboratori Nazionali del Sud (LNS), Via S. Sofia 62, 95123 Catania, Italy

⁴³Nikhef, Science Park, Amsterdam, The Netherlands

⁴⁴Huygens-Kamerlingh Onnes Laboratorium, Universiteit Leiden, The Netherlands

⁴⁵Institute for Space Science, RO-077125 Bucharest, Măgurele, Romania

⁴⁶Universiteit van Amsterdam, Instituut voor Hoge-Energie Fysica, Science Park 105, 1098 XG Amsterdam, The Netherlands

⁴⁷INFN - Sezione di Roma, P.le Aldo Moro 2, 00185 Roma, Italy

⁴⁸Dipartimento di Fisica dell'Università La Sapienza, P.le Aldo Moro 2, 00185 Roma, Italy

⁴⁹Gran Sasso Science Institute, Viale Francesco Crispi 7, 00167 L'Aquila, Italy

⁵⁰University Mohammed V in Rabat, Faculty of Sciences, 4 av. Ibn Battouta, B.P. 1014, R.P. 10000 Rabat, Morocco

⁵¹INFN - Sezione di Bologna, Viale Bertini-Pichat 6/2, 40127 Bologna, Italy

⁵²INFN - Sezione di Bari, Via E. Orabona 4, 70126 Bari, Italy

⁵³Department of Computer Architecture and Technology/CITIC, University of Granada, 18071 Granada, Spain

⁵⁴Géozur, UCA, CNRS, IRD, Observatoire de la Côte d'Azur, Sophia Antipolis, France

⁵⁵Dipartimento di Fisica dell'Università, Via Dodecaneso 33, 16146 Genova, Italy

⁵⁶Université Paris-Sud, 91405 Orsay Cedex, France

⁵⁷University Mohammed I, Laboratory of Physics of Matter and Radiations, B.P.717, Oujda 6000, Morocco

⁵⁸Institut für Theoretische Physik und Astrophysik, Universität Würzburg, Emil-Fischer Str. 31, 97074 Würzburg, Germany

⁵⁹Dipartimento di Fisica ed Astronomia dell'Università, Viale Bertini Pichat 6/2, 40127 Bologna, Italy

⁶⁰Laboratoire de Physique Corpusculaire, Clermont Université, Université Blaise Pascal, CNRS/IN2P3, BP 10448, F-63000 Clermont-Ferrand, France

⁶¹INFN - Sezione di Catania, Viale Andrea Doria 6, 95125 Catania, Italy

⁶²LSIS, Aix Marseille Université CNRS ENSAM LSIS UMR 7296 13397 Marseille, France; Université de Toulon CNRS LSIS UMR 7296, 83957 La Garde, France

⁶³Institut Universitaire de France, 75005 Paris, France

⁶⁴Royal Netherlands Institute for Sea Research (NIOZ) and Utrecht University, Landsdiep 4, 1797 SZ 't Horntje (Texel), the Netherlands

⁶⁵Dr. Remeis-Sternwarte und ECAP, Universität Erlangen-Nürnberg, Sternwartstr. 7, 96049 Bamberg, Germany

⁶⁶Moscow State University, Skobeltsyn Institute of Nuclear Physics, Leninskiiy gory, 119991 Moscow, Russia

⁶⁷Mediterranean Institute of Oceanography (MIO), Aix-Marseille University, 13288, Marseille, Cedex 9, France; Université du Sud Toulon-Var, CNRS-INSU/IRD UM 110, 83957, La Garde Cedex, France

⁶⁸Dipartimento di Fisica ed Astronomia dell'Università, Viale Andrea Doria 6, 95125 Catania, Italy

⁶⁹Direction des Sciences de la Matière - Institut de recherche sur les lois fondamentales de l'Univers - Service de Physique des Particules, CEA Saclay, 91191 Gif-sur-Yvette Cedex, France

⁷⁰INFN - Sezione di Pisa, Largo B. Pontecorvo 3, 56127 Pisa, Italy

⁷¹Dipartimento di Fisica dell'Università, Largo B. Pontecorvo 3, 56127 Pisa, Italy

⁷²INFN - Sezione di Napoli, Via Cintia 80126 Napoli, Italy

⁷³Dipartimento di Fisica dell'Università Federico II di Napoli, Via Cintia 80126, Napoli, Italy

⁷⁴Dpto. de Física Teórica y del Cosmos & C.A.F.P.E., University of Granada, 18071 Granada, Spain

⁷⁵Université de Strasbourg, CNRS, IPHC UMR 7178, F-67000 Strasbourg, France